UNIVERSITEIT TWENTE.

COMPARISON OF SENSING ELECTRODES FOR COATING ASSESSMENT

Part of deliverable D1 of the NTP “Development of Sensor Technology and Maintenance Concepts for Corrosion-related Maintenance”

COLOFON

DATUM
23 December 2020

VERSIE
1.2

STATUS
final

AUTEUR(S)
Gergely András

TELEFOON
+36702721994

E-MAIL
a.gergely@utwente.nl

POSTADRES
ET-AM
Postbus 217
7500 AE Enschede

WEBSITE
www.utwente.nl

CONTENTS

SUMMARY

In this report, a technology assessment on the various options for performing corrosion-protective coating degradation assessment is performed, specifically focusing on the sensor type and electrode configuration. A comprehensive literature survey is made on currently available sensing configurations. Then the iterative process of electrode selection and testing is described, ultimately leading to the assessment of two prototype electrodes: the interdigitated strip-line and concentric array configurations.

1 INTRODUCTION

In the PDEng project on corrosion sensors, part of the Defence Technology Project (DTP) “Corrosion Sensors”, several sensor concepts and configurations are developed and tested. This document describes the literature study and the (iterative) process to select the most suitable sensor configuration. A summary of this process will be included in the PDEng thesis, for the details the reader will be referred to this document.

The outline of the document is as follows: in section 2 the motivation for the first preliminary type of (wire-based) sensors is given, which are then discussed in more detail in section 3. As these sensors have some drawbacks, a 2nd generation of sensors is developed. These planar configuration sensors are discussed in section 4. In section 5 two types of planar sensors are detailed further till the level of prototype sensors. Finally, section 6 provides the summary and conclusions of this study.

2 MOTIVATION FOR WIRE-BASED ELECTRODES

Ballast tanks of naval ships contain sea water for up to 30% of the entire cruising time and over that period coatings experience immersion type exposure [1]. The surrounding sea water as a conductive electrolyte regardless of temperature fluctuation between ~5 and 12.5°C offers the means of electro-chemical sensing to CM, using metallic (primary) electrodes immersed in the ionic conductor. This idea is supported by the widely accepted rapid coating assessment method based on EIS used by societies of electrochemists [2–4] and corrosion engineers [5–9]. As a further proof, the expert contractor in the DTP, Endures BV, also utilizes this technique in a variety of ways for inspection both in the laboratory and in the field.

This is a chance and limitation in itself at the same time. It is a chance because the unavoidable presence of seawater allows coating characterization with generally acceptable accuracy, whereas limitation because coating condition assessment cannot be performed without electrolyte. The wire-based electrodes are thought to represent a practical advantage over monolith planar electrodes in a sense of flexible and reliable operation under varying water level and diverse substrate geometries, which may not be attainable by the planar electrodes. In the next section, some types of wire-based electrodes are proposed and tested.

3 WIRE BASED PRELIMINARY ELECTRODES SUITED FOR TESTING UNDER IMMERSION

Preliminary sensor electrodes were created in many shapes and sizes from tin coated copper wires of two diameters. All electrodes were hand-made. Most of them were prepared in pairs with nominally the same geometry for the sake of joint assessment of the electrodes via applying those on the same coating. The main electrodes were formulated in spiral and meander shapes in 3 different sizes, but due to brevity of time only two larger in size were tested. Images of wire-based electrodes are presented in Figure 1.

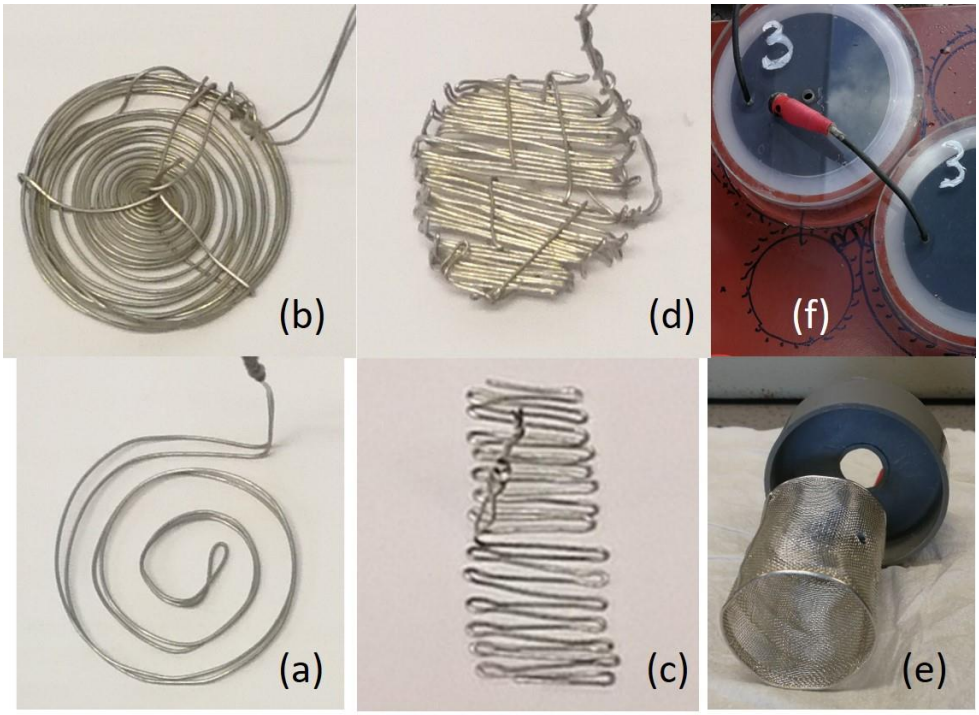

FIGURE 1. IMAGES OF THE PRELIMINARY TYPE ELECTRODES ALONG WITH THE REFERENCE TYPES: THE EXTENDED SPIRAL (A), THE LARGE SPIRAL (B), DOUBLE MEANDER (C), EXTENDED MEANDER (D), PLATINUM GAUZE (E) AND THE PLANAR CARBON ELECTRODE (IN PMMA HOUSING, F).

The spiral and meander shapes were aimed at investigation. It is because the former is similar to loop coils used for eddy current testing of steel substrates underneath coatings, whereas the latter provides effective sensing of coating electrical properties, i.e., conductivity and permittivity with sufficient sensitivity and without any inductive response arousal in the measured impedance signal. It must be noted, single- and double-wire spiral electrodes are not expected to model inductivity of wire-loops (used for inductive sensing) due to lack of continuous high current transmission in the conductor from forward to backward leads (or ‘up’ & ‘down’ turns of loops) but served as surrogates to analyse impedance responses arousal from the coating. The meander shape is regarded as linear alternative to the spiral alignment, featuring a transition between the ideal monolith planar electrode and the highly distributed spatial type wire-based configurations. Then, results were compared to outcome obtained with the ‘reference’ type planar electrodes. There were two ‘reference‘ type electrodes in use. The cylindrical platinum gauze (Figure 1e) was one reference type for laboratory testing, and the PMMA housed planar carbon electrode (diameter of 10 cm) was the other reference (Figure 1f). Comparison between and the scale of departing test results as obtained with the wire based electrodes and the ‘reference’ ones provided the basis to accept

or dismiss a certain concept of sensor electrodes. Since many electrodes were created with various geometries, this number combined with the variation in independent variables resulted in an extensive test matrix which could not be addressed completely. From an electrochemistry viewpoint, the tin plated copper wire was sufficiently corrosion resistant to perform coating assessment and at the same time does not feature high charge-transfer resistance or polarisation resistance (~103 ohm cm2) which could be invalidating for pore resistance assessment. Therefore, these electrodes were used for AC and small vertex potential DC tests. Geometrical details of the wire electrodes are given in Table 1.

TABLE 1. MAIN PROPERTIES OF THE HAND-MADE PRELIMINARY SENSOR ELECTRODES

Electrode types	Wire & geometrical diameter (mm)	Complete length (immersed zone, mm)	Number of wire arms	Surface (cm^2)	Surface ratio (m^2/m^2) to		Estimated geometrical cell capacitance [ii] (F)	Estimated electrical double-layer capacitance [iii] ($\mu F\ cm^{-2}$)
					Coating area	Pt gauze		
Investigated configurations								
Double meander (DM)	0.5	490	2	7.7	0.78	0.14	4.03×10^{-10}	154
Extended meander (EM)	0.5	1500	2	23.6	2.38	0.43	1.23×10^{-9}	471
Extended spiral (ES)	0.5	245	2	3.9 (7.7 [i])	0.39 (0.78)	0.14 (0.07)	5.53×10^{-11}	77
Large spiral (LS)	0.5	1700	1	26.7	2.70	0.49	3.83×10^{-9}	534
Reference configurations								
Pt gauze (cylinder)	35	50	-	55	5.55	1.00		1100
Carbon (planar) plate	35.5	Complete	-	9.9	1.0	0.18	1.71×10^{-11}	198
Carbon (planar) plate	80 [vi]	Complete	-	50.3	0.64	-	8.67×10^{-11}	1005

[i] Native geometrical surface is also given although effective surface were lower due to close reeling of wire pairs, so double-wire data given in parentheses.

[ii] Cell capacitance was estimated based on permittivity of sea water (ε_r=78) at room temperature and using engineering calculation methods [10]

[iii] Double-layer capacitance of the electrodes were calculated based on double-layer capacitance of carbon electrodes immersed in sea water [11]

[vi] The coating surface area tested with the large PMMA-CE type electrode was 78.5 cm^2 with inner diameter of 100 mm and the cell capacitance was derived for electrode-coating distance of 40 mm.

All electrodes were fixed at a distance of ≈30 mm from the coating surface, except for the platinum gauze those closer perimeter was at a distance of ~5 mm.

As it is summarised in Table 1, except for the ES the ratio of geometrical surface of the preliminary electrodes and the investigated coating area was close to unity, with the DM electrode being surpassed far by the EM and LS electrodes. Compared to the platinum reference electrode, LS was the closest in surface area. Small differences in geometrical surface area translate into excessively large cell and double-layer capacitance of the test configurations due to volumetric alignment of the electrodes and the presence of sea water. The EM and LS electrodes featured high cell and interfacial capacitance, exceeding far the DM and ES and standard electrode configurations. Despite the large lateral size, low and moderate contribution to these

characteristics of the monolith planar reference electrodes is a definite advantage. These properties suggest incapable representative assessment of coating capacitive characteristics by the wire electrodes. On the other hand, increased size and/or lower charge-transfer resistance of the counter electrodes can offer a more representative estimation of the coating resistance via two electrodes test setup, owing to the decreasing additional resistance measured in series with the coating in the test circuit. Therefore, wire-based electrodes are regarded as alternative means of assessment of coating resistance, more exactly the pore resistance but these may never be recommended to use for evaluation of coating capacitive character. To support this in general, coating resistance is always referred to as a more sensitive parameter / indicator of coating condition rather than capacitive properties.

From a practical viewpoint, inner capacitance of the meander configurations remained moderate along with lower variation (based mainly on length of the wire arms), closer to each other than the spiral configurations, owing to the steady distance within arm segments almost independent of the covered geometrical area. In an evaluation, the LS with 25 turns over a diameter of 40 mm leads to large cell and double-layer capacitance which is the least favourable due to the high base, own capacitive signal and so low proportion of the useful signal such as permittivity of the coatings. Although large cell capacitance would mean high rate of interacting surface between electrodes and coating surface, unfortunately this translates to high double-layer capacitance as well. This is the main reason why wire-based electrodes are not used for laboratory test setups.

Based on the experimental results carried out in the first design cycle, pore resistance of the coating/steel samples obtained with various electrodes by both AC and DC test modes are summarised in Figure 2. The DC (linear polarisation resistance, LPR) and AC (electrochemical impedance spectroscopy, EIS) test modes provided moderately varying results with the coatings similarly to the outcome obtained with the different electrodes by the same technique. After an initial 240 hours of immersion exposure, in most cases impedance test results indicated higher pore resistance with greater STD than DC (LPR) data except for the salted sample (III), regardless of the electrodes. In other words, it is interpreted that impedance testing of coatings in early immersion stage is less sensitive to pore resistance variations in comparison with the DC type LPR technique. Explanation to this phenomenon is twofold. Firstly, the time constant of micro-pores is assessed above 1 Hz and so above the threshold of full penetration of the oscillating electrical fields into the pores of mildly hydrated coatings (≤10^3 Hz). Secondly, the generally large distance of working/reference and counter/sensing electrodes coupled via a relatively high electrical resistance and the electrical shielding effect (permittivity) of the electrolyte leads to low sensitivity of detection of the pore resistance. This shortfall is known as frequency dependent penetration depth [12–16]. This is interpreted as effective screening details of material properties in a distance against detection sensitivity. On the other hand, surface area and charge-transfer resistance of the electrodes plays only an inferior role in the assessment of pore resistances. Nearly in all cases, the direction of deviations by the wire-based electrodes was the same from the reference, as pore resistance was always overestimated in comparison with the reference setup. In general, the sensing capability of the wire-electrodes was in line with the expectation not departing markedly from each other and from the reference. Nonetheless, deviation in data obtained by the various electrodes were generally larger than the variation scale of the coating-specimen samples, which is unacceptable for an accurate and reliable assessment of coating condition. This is despite the fact that the impact of surface treatment cannot be evaluated sensitively by the wet chemistry technique in the initial immersion stage.

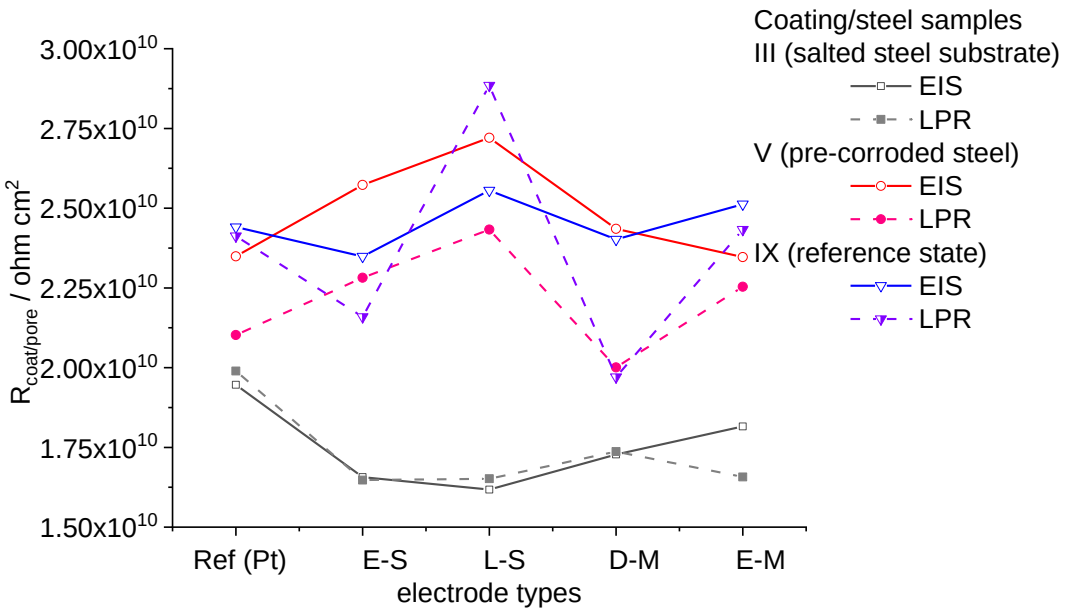

FIGURE 2. PORE RESISTANCE OF ALL THREE TYPES OF COATING/STEEL SAMPLES DERIVED FROM IMPEDANCE AND LPR DATA (AT 240 HOURS OF EXPOSURE OF THE PRELIMINARY TESTED 'THICK' COATINGS).

Relative differences in data measured with the AC and DC techniques are summarised in Figure 3. The largest differences were noticed with the LS and DM electrodes when neat coating and pre-corroded steel substrates were investigated. These two conditions are the main focus during maintenance to assess properly, so it was concluded such electrodes must be omitted from serious consideration for further development.

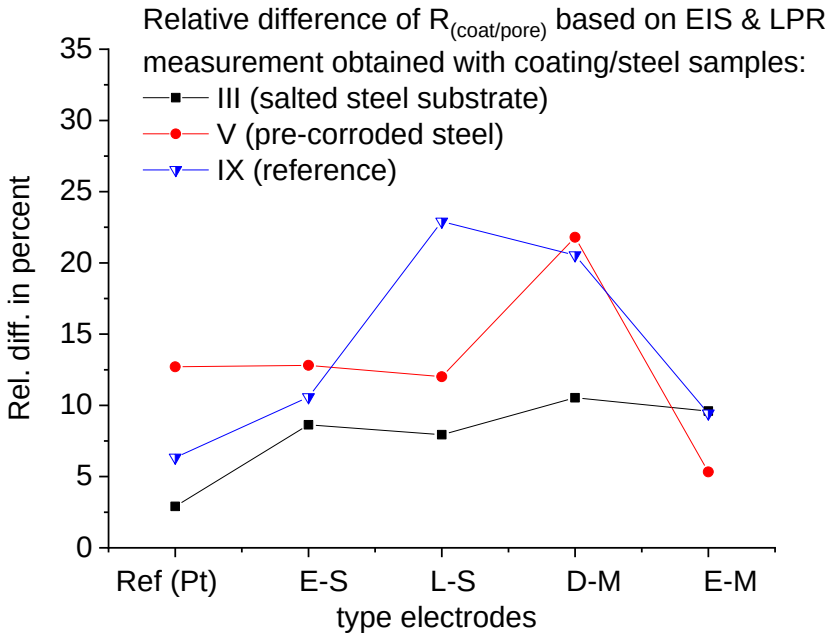

FIGURE 3. RELATIVE PERCENTAGE OF DIFFERENCE BETWEEN PORE RESISTANCE OF COATINGS OBTAINED WITH IMPEDANCE AND LPR TESTING TECHNIQUES.

This performance parameter shed light on invalidity and unreliability of the sensors readings in a sense to provide credible and valuable information to maintenance personnel. Overall, the EM provided results with generally the lowest deviation from the reference setup and variation.

When the quality of AC and DC test results are regarded separately, then data of relative difference summarised in Figure 4 gives unambiguous insight into performance metrics of the electrodes. Pore resistance measured with the ES and LS indicated much greater difference by AC and DC testing modes, respectively, than the results obtained with DM and EM electrodes. Focusing further to meander type electrodes, EM seemed to perform unanimously better than DM. Overall, the EM provided the lowest differences in EIS (AC) test mode and performed well in LPR (DC) mode. As an inherent inference, electrode geometry proved to be highly influential on sensing pore resistance, beyond the variation of material properties even in case of good coating condition. From another viewpoint, the EIS technique is more sensitive to the geometry of the electrodes on sensing performance. Hence, owing to the preferential application of this impedance test mode of the coatings in the field, definition of a proper electrode geometry is utmost importance for suitable implementation.

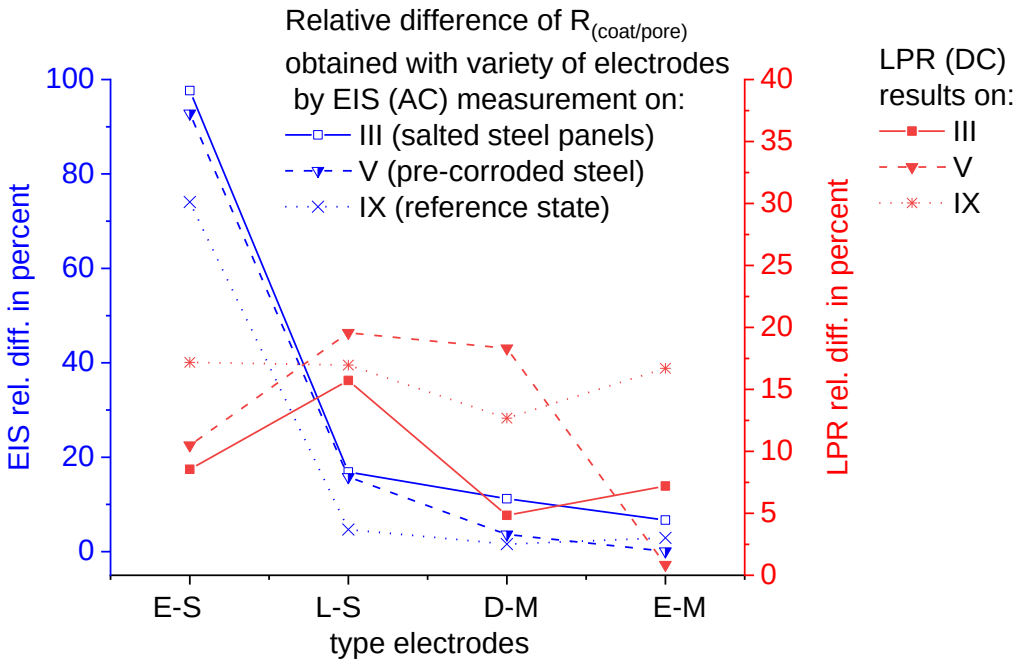

FIGURE 4. PERCENTAGE OF RELATIVE DIFFERENCE OF PORE RESISTANCE OF COATINGS OBTAINED WITH IMPEDANCE TESTING MODE COMPARED TO THE RESULTS OBTAINED WITH THE REFERENCE PT GAUZE ELECTRODE.

To reflect on the shortfalls of the presence of electrolyte, and its impact on sensor data and on derived material properties, the pore resistance and the coating capacitive properties obtained from the reference electrode based one- and two-cell configurations are summarised in Figure 5a and b. Generally with all three types of coating/steel samples, increased pore resistance was estimated based on the one-cell test configuration compared to the two-cell setup. After deduction of resistance elements in series, it can only mean contribution of the polarisation resistance, and or pure the charge-transfer resistance of the testing carbon electrode. Thus, this component must be around 10^3 ohm cm^2, orders of magnitude lower than the coating resistance and decrease by 10^2 times after normalisation to unit surface area, it is still not enough to gain entirely distortion free pore resistance of the neat coating (1.1, Figure 5a).

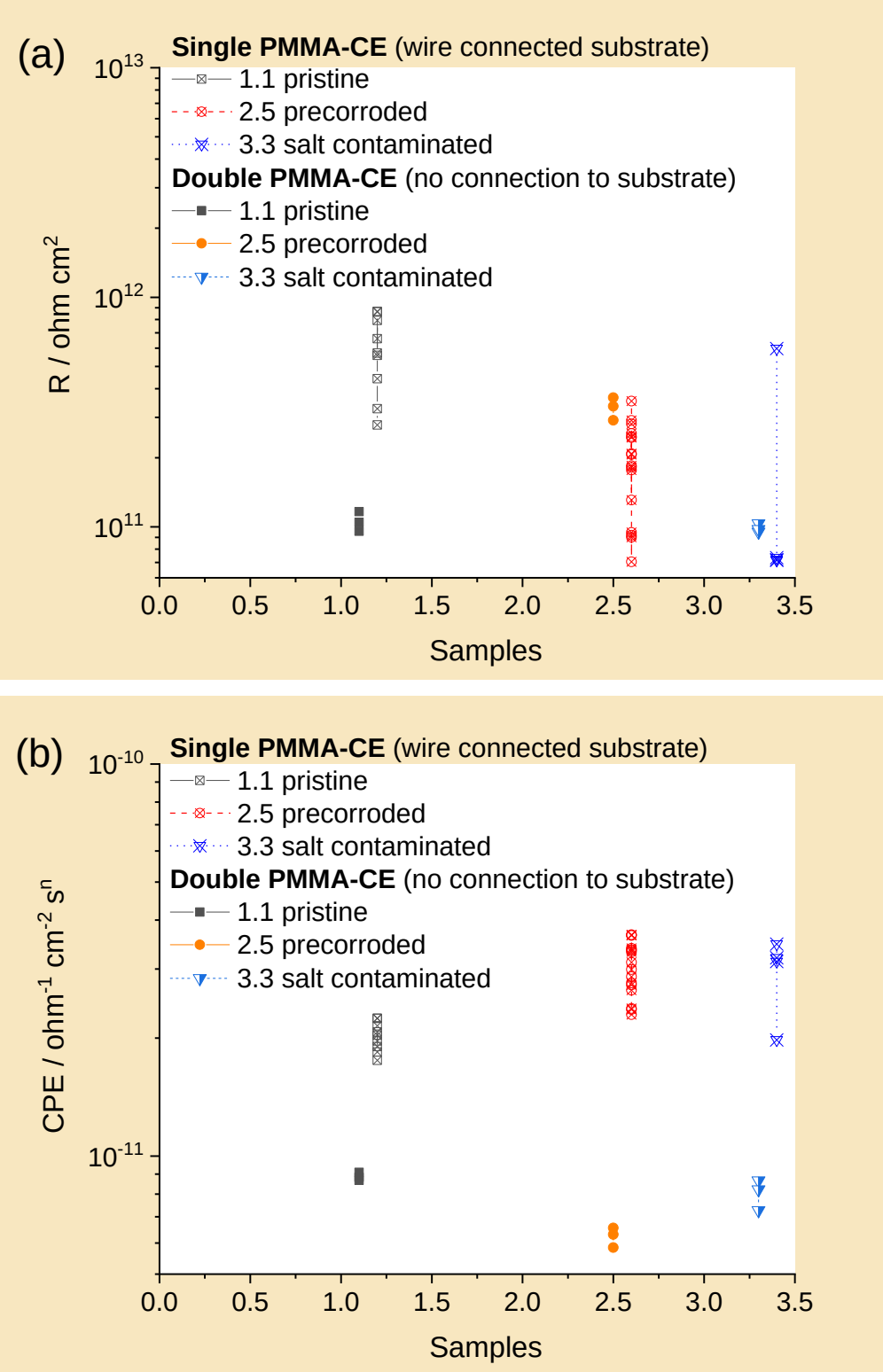

FIGURE 5. COATING RESISTANCE (A) AND THE CONSTANT PHASE ELEMENT (B) DERIVED FROM DATA OBTAINED WITH THE SINGLE AND DOUBLE PMMA-CE PLANAR ELECTRODE TEST SETUPS WITH AND WITHOUT CONNECTION TO SUBSTRATE, RESPECTIVELY. SAMPLES WERE THE 'BLACK COATING' PANELS PREPARED IN THREE DIFFERENT STATES: PRISTINE (1.1), PRE-CORRODED STEEL SUBSTRATE (2.5), SALT CONTAMINATED STEEL SUBSTRATE (3.3).

Aside from the perfect initial condition, if a correction could be plausible to fix counter electrode contribution then one must consider the entirely different conditions of the pre-corroded (2.5) and the salted specimen (3.3) samples and the obviously different correction factors can be deducted by comparison of the two test cell configurations. Although such a marked difference in the result is not expected with the two-cell setup at least at the beginning of immersion test, in a later phase of exposure with increased moisture take-up the markedly decreased coating resistance certainly lead to inaccurate estimation of coating properties while extraction of parameters relating to coating properties performed. In accordance with the theoretical expectation, absolute range and the scale of deviation in the coating capacitive character becomes also error loaded by the high double-layer capacitance on the opposite test electrode (Figure 5b). It is worth noting, in this regard, opposite trend of correction is recommended to perform as increasing rate of conversion of the coating capacitive character would erroneously occur along with the progressively deteriorated condition of the coating and steel substrate. This means correction of wet condition data to reference type dry test results is by good chance always condition dependent. Without a reference for validation, then proper correction can easily be missed.

Further results with the planar electrodes in the preliminary design stage revealed limited validity and credibility of the wet phase material testing and the two-cells without wire connection to substate configuration. The latter is due to the limited electrification of the coating through the electrolyte and the very difficult plausible fitting of the impedance spectra obtained by the double-cells setup to the DC range. In addition, the averaging effect of the two cells areas always means an added limitation, possible distortion of the real coating condition over the specific macroscopic areas. According to reference data of epoxy sheet materials, in initial phase of the immersion test, coating or pore resistance of coal-tar pitch epoxy paint coatings must be around 10^{10} ohm cm^2 at 200 µm DFT, which means 10^{11} ohm cm^2 / 1 mm coating thickness at 0.1 Hz [17], which is in very good agreement with results obtained with the double-cells setup.

To tackle the observed drawbacks of submersed testing with wire-type sensors, the next design iteration focuses on dry-phase testing with planar type electrodes. Careful evaluation of data obtained with the monolith planar carbon electrodes is discussed in the next section by comparison with the results obtained with the proposed prototypes. This serves the justification for dry test configuration rather than the electrochemical wet setup.

4 DRY PHASE TESTING WITH PLANAR ELECTRODE CONFIGURATIONS

The solutions to the aforementioned problems can be manifold. However, the options in the DTP were restrained to certain historically already proven industrial solutions such as sensing with in-plane coplanar electrodes. To be more specific on the physical embodiment, open-ended strip-line and concentric electrodes were opted for sensing with bending electrical fields. In addition, such shift in the concept was also in line with the programmatic design requirements. As for point probe material testing, the four-point contact mode measurement is a proven standard technique, but accurate resistivity assessment requires a high voltage, controlled laboratory or at least noise-free environment and careful correction [18] according to the test bench configuration and spatial ratio of the tested materials [19–24]. Therefore, attention in the following is focused on electrode configurations associated with real potential to field applicability.

4.1 Generic aspects of the parallel plate setup

a) According to the reference design by Lord Kelvin [25], traditional electrode configuration utilises two concentric disks and a ring guard electrode, from which the latter works for shielding, to test dielectric permittivity, energy storage properties in response to the electrical field, conductivity and dissipation susceptibility of the materials. This setup leads to emerge of the highest attainable homogeneous electrical field distribution inside the disk-confined volume range and with the least bending effect around edge of disk and concentric electrodes [26] by mainly excluding the bending field out of the sense electrode. Thus, any effect after bending of the electrical field can be minimised by the outer grounded shielding electrode [27,28]. This configuration is the best approximation of ideal circumstances, reference setup to characterise materials. Depending on the frequency range of testing and the material properties, two, three and four electrode configurations exist to eliminate polarisation effects and increase sensitivity of detection [29,30]. Nevertheless, in reality, the electrical field and the resulting current do not homogeneously distribute laterally over the disk electrodes surface [31,32]. Instead, the electric field bends [33] and concentrates along edges, at perimeter and decrease towards centre of disk plates [34]. This is the reason why the effective electrode surface needs correction. Material properties can be uniquely identified and characterised by variation of three parameters such as distance of electrode plates, temperature, test voltage and current settings over the interested frequency range. To obtain exact data via accurate material characterisation, results must always be corrected to the edge effect between driver and sense electrodes depending on the ratio of gap between sense and guard electrode, and distance of the electrodes, thickness of the tested materials [35]. In the aspect of inspection and monitoring, the reference electrode configuration may only be sensibly used with the lowest implementation flexibility for field applications, but is rather genuinely suited for laboratory test under controlled condition.

b) Electrochemical implementation of traditional electrode configuration boasts some pros and hides some compromise as discussed before. Traditional electrode configuration with two functional test electrodes is widely used for testing paint coatings [1,2], in which the third electrode serves as reference or quasi-reference electrode to set free-floating potential of the investigated electrode and the electrically connected, tested material. These setups involve one coated (working) electrode and one uncoated counter electrode. Despite the practical convenient feasibility to perform rapid condition assessment in an situ way, this setup hides some marked compromises such as the high interfacial pseudo or double-layer capacitance of uncoated counter electrodes (~20 F cm^{-2}) which is many orders of magnitude higher than the capacitive response of the coatings based on electrical permittivity. In addition, interfacial resistance of the counter electrode for charge-transfer, which is coupled in series in the measurement circuit, can have varied extent of erroneous effect on the estimated coating resistance. Variation of the counter electrode surface area may not offer viable remediation

due to the following reasons. When electrode area is set smaller, then double layer capacitance decreases and resistance contribution of the counter electrode (as combination of charge-transfer resistance and surface area) to the material tested with the work electrode would increase. Furthermore, surface area of the coating would not be effectively fully tested with restrained distribution of the electrical field owing to the moderate distance and conductivity of the electrolyte and so fast decay of electrical field strength occurs from counter electrode in proximity of the material [36]. When counter electrode surface is increased, then series resistance in the measure circuit is reduced and the entire coating surface is affected by the electrical field but the double-layer capacitance would be excessively large to cancel constant phase element behaviour of the work electrode tested material (paint coating). In a validated case, corrections based on counter electrode characteristics may provide a sufficient solution.

c) Impact of many of the aforementioned shortages can be reduced by applying symmetrical setups, characterising nominally the same material with both electrodes. Traditional reference test setup used by Endures BV adopts this intention. Thus, similarly to the test configuration of 'no connection to substrate' type electrochemical noise test configuration, this effectively addresses the need for nominally the same coating CPE behaviour and series resistance in the measure circuit. Some limitation may also arise in this case such as restrained electrification, electrical activation of the coatings by the shielding electrolyte, screened distant electrodes and the detected possibly increased current between the electrodes due to additional electrochemical reactions may occur on both uncoated, not fully blocked (passive), reflective electrodes. In addition, further difficulty may be encountered with representative evaluation of impedance spectra, correct extrapolation to the unknown DC range. Definition of material properties of individual parts in the combined spectra is genuinely questionable if not almost impossible to resolve. The latter can itself lead to markedly compromised and erroneous assessment of material properties, i.e., individual macroscopic coating areas. Strength of the technique is the high flexibility for field application and the acceptable rate of material characterisation, moderate performance of testing rate of samples, throughput of the method aside from the sometimes required some days long pre-hydration of the investigated areas. Corrosion engineers and material scientist use this type of testing due to high in situ implement-ability and the unnecessary interruption of exposure tests.

4.2 Practical coplanar electrode configurations

Traditional electrode configuration with parallel plates of monolith structure can hardly be used for field type material characterisation. Therefore, open geometric electrode structures, primarily coplanar configurations are applied with an aim to combine electrode pairs for coating testing under real-life modelling condition. Functional analysis of these electrodes and their use in electrolyte is justified by the following reasons. The DTP is interested in all technical solutions which can be adopted to test dry and immersed paint coatings and effectively used both in the absence and presence of aqueous electrolyte. Thus, versatility of the use case with test electrodes is utmost for monitoring type application.

On the other hand, inspection use case can either be performed with immersed or bare electrodes. For the immersed use case, meander electrodes may meet usability and feature genuinely compatible solution due to the need of electrolyte involvement for coating characterisation. What is advantage on one side, shortage on the other. Such open electrode configurations are reliable under continuously changing scenarios, e.g., immersed and non-immersed conditions but feature relatively large surface which makes effective material, coating testing. This can be a monitoring solution over a quarter of service time. For rest of the time, electrode configurations must be implementable and perform well under atmospheric condition, with the meaning of surrounded with air of high relative humidity. This necessitates high bending of the testing electrical field, anywhere in between around 90 and 270 degree, between the individual electrodes. Theoretically, the least bending is favourable but a certain level of spatial openness between electrode pairs is required for sensible applicability of probes. Therefore, most of the applications prefer using coplanar electrodes with a variety of in-plane geometries. Next, the properties and performance of these electrode configurations are discussed.

a) **Meander, spiral and interdigitated type electrode in-plane geometries**
Various in-plane electrode geometries were tested and reported in the literature. Rectangular configurations like square-shaped, maze, spiral and comb electrode patterns are the most abundant [37]. These proximity sensors measure very low capacitive character expressed in fF and pF, which can be difficult to extract from background noise loaded signal in case of the test performed with high resistive coatings at maritime field. The fringing field assessed capacitive character depends on many factors such as the sensor size and geometrical pattern of the electrode strips. As an example to the latter, from the maze, spiral and comb patterns the latter two, especially the spiral proved to be the most sensitive at a cost of shortened linearity range of sensing (rapid saturation) in comparison with the comb electrode pattern. Electrode width and gap, and height of the dielectric media has primarily impact on impedance in the conductor transmission line [38]. Thus, increasing impedance and decreasing phase velocity in the response signal is affected by, i.e., moisture, water uptake. Simple strip configuration can be useful to test condition of coatings on cylindrical structures [39]. From the interdigitated type spiral and concentric sensors specified for NDT sensing [40–42], enhanced sensitivity of the interdigital configuration was found in comparison with the traditional simple disk-ring planar and coplanar electrodes type capacitive sensor configurations. Moreover, IDE type configurations can also provide higher SNR and better accuracy in materials characterization due to more concentrated electric field in between electrode pairs, higher density and spatial resolution of material testing. Nonetheless, simple disk-ring configuration features deeper penetration depth and better immunity to lift-off variations. The latter may be more important for effective and reliable maritime implementation. Linear response to change of materials dielectric was obtained within a narrow range (ε_r=2−6). From the many coplanar electrode configurations, open-ended linear microstrip lines are the most common and studied, since this alignment was opted for investigation in the intermediate design stage. Inferences can be overviewed as follows. The concept of edge-coupled microstrip lines implemented in the form of interdigitated electrodes can be a proper sensor hardware solution to characterise properties of materials featuring low electrical conductivity and permittivity, with some important stipulations. These stipulations involve short and proper wiring of the sensor electrodes if composed of many smaller blocks aligned in any array topology. If there is a single large electrode block without array formation in-plane then parallel connection would not lead to suppressed sensitivity and reliability of detection. In addition, the main feature size, width and spacing of the electrodes of the interdigitated configuration must be closely comparable with the interested penetration depth, thickness of the tested materials over the metallic substrates. This ensures sufficient sensitivity of the edge-coupled electrodes to interaction of bending electrical fields with the surrounded material for valuable sensitivity while obviating air-gap caused accidental decrease of sensing performance [43]. As a summary, despite the experiments, promising results with some aqueous test media and the numerous attempts to obtain positive results with the small size IDE type mono- and array configurations, no entirely coherent and credible results were gathered with the model type maritime coatings. This disappointing finding was later realised confirmed by reviewed literature as interdigital impedance sensors are not found favourable for material characterization due to difficulties by the presence of lift-off air gaps [44]. These implementations may face special complications while surface of high resistive materials from IDE measurement data attempted to derive. There are many factors on which readers may be advised to refer on the literature discussing such issues which not fully be resolved until most recently [45,46]. Further shortage of this electrode configuration is the compromised accuracy by flexible application. Deformation of the sensor platform on the electrode located metallisation side is not allowed after all as that sensor electrode geometry responsible for detection characteristics and performance.

For engineering safety reasons besides some research ambition in the DTP, contact mode testing with concentric type electrode configuration was also attempted to test with model maritime coatings. This was the case despite characterization of high resistance materials with contact mode is pretty complex. The dominant role of the electrode edge

in current injection was recognised and high variation of degree of surface and bulk current components found during testing high resistance, insulating materials, depending on type of material and electrode probe geometry and surface preparation [47]. Thus, bulk and surface components, i.e., absorption and resorption currents can be spit in share depending on test parameters. Surface component depends on surface condition which can be traced back to surface treatment, preparation, although its time dependence does not differ much from the bulk component.

b) **Concentric type in-plane electrode geometries**
International standards and high profile companies offer well developed engineering solutions [48] to test resistivity of materials with coplanar concentric sensors. Beyond those, there are plenty of applications for dielectric testing mainly at the field of life-science such as in-vivo stripping of chemical agents [49] , skin hydration [50–52] and characterisation [53], moisture [54] and hydration sensing [55,56] in soil [57,58], proximity, touch and pressure sensing [59] using flexible platforms with non-metallic, carbon conductor [60]. Skin resistance [61] with its moderate resistance (1 Mohm) is characterised over wide frequency range between 1 kHz (with uniform potential distribution along the radius) and up to 1 MHz [62]. Furthermore, concentric sensors are preferentially used for multi-layer materials [63] in electro-physiology sensing, i.e., electroencephalography, electromyography, electrocardiography [64], detection of emboli in vessels [65]. Customisation for electrocardiography monitoring, bilayer design of concentric ring electrodes is proven to be the most sensitive probe alignment in the moderate resistance range [66]. Flexible patch probes allow spatially focused stimulation [67]. On theoretical, parametric estimation of such probes are well established [68] and according to the literature, the concentric ring design works as a Laplacian filter, 2nd spatial derivative of measured potentials, underscoring the changes in state of electric dipoles and so effectively differentiate closely spaced dipole sources [69,70]. An important stipulation, practical implementation of concentric type multi-polarity filters requires dry interface [71,72] for the sake of high spatial resolution and good signal-to-noise (SNR). Due to the universal very good reference of the concentric sensor probes in the literature, one of the detailed design physical embodiments was opted to accommodate this electrode alignment. General advantage of this configuration in comparison with the open-ended strip-lines, e.g., interdigitated or interlaced linear-strip sensors is the enclosed electrode formulae and by that the shielded sense electrode from the outer electrical noise. In part, these are the reasons why standards recommend this electrode alignment for both field and laboratory applications.

c) Electrode arrays
As it was experienced during the intermediate design stage, no array simple formation of the strip-line electrode configuration is advised if not carefully and thoroughly optimised. This was the main conclusion despite the fact array formation of single probes is known to enhance proportionally the detection sensitivity along with steady SNR. This issue was treated in a way to increase lateral surface of the strip-line electrodes as much as allowed by the application. As for the concentric probe design, material test in contact mode also improves by the increasing number of sensing units. Thus, the concentric probe was designed to form an array with large number of single units. In optimal case, there must be a single, unique cell constant (directly linked to electrode alignment of the single unit) to estimate resistivity of materials.

d) Capacitive imaging
Capacitive imaging term is used for all sensing solutions which exempt of direct contact of the sensor probes with the tested materials. In this aspect, all fringing field sensors feature such applicability, but sensitivity and robustness of detection varies largely with the electrode alignment and probe embodiment. This is a relatively new sensing operational mode mainly achieved by coplanar electrodes. In a wider overview to reflect the high versatility, interdigitated electrodes were first generation capacitive imaging and tomography sensors [73]. Then similar electrode configurations were adopted for proximity,

touch and wearable sensing [74–76], i.e., capacitive fingerprint sensors use array of fringing field sensors for in-vivo & in-situ measurement. Successful use of IDE type probes for dielectric sensing is connected to industrial applications like sensing chemical species [77], monitoring manufacturing processes like polymer curing [78,79] and compounding [80], sensing relative humidity and time of wetness [81], chemical species in gas [82], security check [83], electroanalytical detectors [84], dielectrophoresis [85], energy harvesting [86], supercapacitors [87], lab on chips [88,89] to impedimetric sensing [90], detection of bacterial cells [91]. On fabrication of low cost capacitive imaging sensors, reader is advised to refer to the following material [92]. In the viewpoint of early comprehensive investigations, capacitive imaging with IDE type probes for resistance and permittivity detection provided to be sufficiently accurate [93]. Then, sometime later analytical and numerical methods were developed to calculate potential distribution and change in admittance of the probe caused by presence of the dielectric materials as a function of lift-off [94]. To compare interdigitated and concentric type electrode configurations, the concentric probe design is the more favourable electrode configuration according to the literature [95]. In addition, inclusion of a grounded guard electrode between the driver and sense electrodes can always be favourable for both contact and non-contact mode sensing.

e) Non-metal based probes

If additive manufacturing is available to use disposable electrodes for over long-term service, then non-metallic electrode based sensor production would mean further merits to sensor development in the DTP in the sense of cost efficient, environmental friendly and more sustainable solution. There are examples for 3D printed thin and flexible dual and concentric electrodes in which conductor tracks are made of graphene ink, or graphene [96], and applied with adhesives on top of the materials. These sensors are used in the range of 10^3 ohm impedance and frequency of 1 kHz and 1 MHz with power rate of 1 mW at a current uptake of 5 mA. These electrodes were stable in continuous service for sensing over 9 weeks while showing similar performance metrics in the end. By fixing sensors on the human body and being resistant to frequent deformations, continuous electrocardiography monitoring is attainable by textile based concentric ring probes [97]. This can be a good example of customisation of highly deformable CM sensors.

5 FIRST PROTOTYPE DESIGNS IN THE DTP

Based on the results from the previous design iterations, two prototype sensors have been defined: a interdigitated strip-line sensor and a concentric array sensor. The design of these two sensor concepts will be discussed below.

5.1 Interdigitated strip-line sensors

Interdigitated microstrip-line or simply interdigitated electrode configuration is universally applied for capacitive sensing in the industry. Advantages of the electrode configuration are the easily and arbitrarily changeable electrode dimensions, i.e., length and width as well as gap between the electrodes, which parameters primarily responsible for sensitivity of detection and penetration depth, the main range of sensitivity in the tested materials. Sensitivity, the slope of sensor response signal increases steeply with decreasing distance of the electrodes. As an analogue with the parallel plate configuration, the high scale of confined space between the electrodes makes this configuration favourable, whereas in most cases the only single-side, active electrode area utilised for sensing is a shortage. The latter reduces sensitivity overall to less than to around half of the maximum attainable limit. This shortcoming can be properly addressed by thin layer active backplate shielding as it is already well known in the literature.
Front-side view of two interdigitated electrodes with different feature sizes, tested for electrical sensing in one of the DTP design cycles for electrical sensing is presented Figure 6.

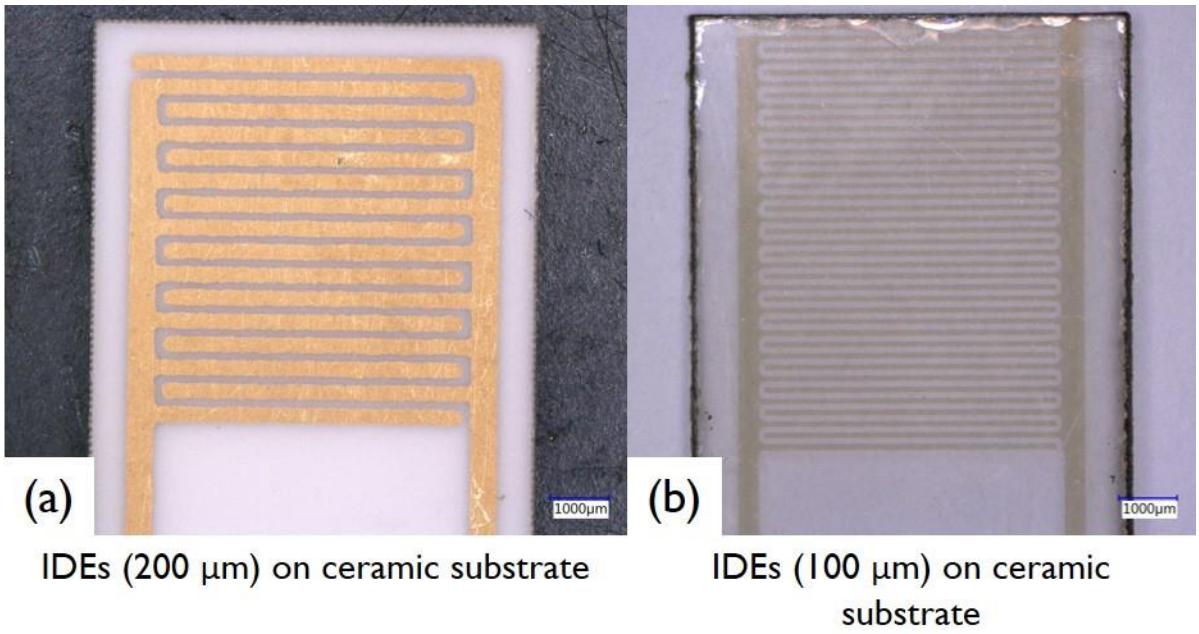

FIGURE 6. FRONT-SIDE VIEW OF INTERDIGITATED ELECTRODES WITH NOMINAL ELECTRODE WIDTHS OF 0.2 MM (A) AND 0.1 MM (B) DEPOSITED ON CERAMIC AND POLYMER SUBSTRATES, RESPECTIVELY.

An ever green research objective has long been to define electrical field and potential distribution in normal direction to, out-of-plane volume region of the electrodes, along with the attainable capacitive response for sensing applications. In addition, in another viewpoint, impedance and capacitance definition of such electrode pairs and multiple tracks, micron-size transmission lines have always been under intense focus due to optimization of printed-circuit boards and

microelectronics. To interpret the mathematical problem in the process to find solution for calculation of bending electric fields over coplanar conducting tracks, electrodes are given in Figure 7, in which initial step is called conformal mapping leading to solution. Based on numerical methods, simple finite element modelling (FEM) can only provide approximate solution of the system under study as represented in Figure 8. Low detail level in system definition and modelling engine leads to highly approximate solution in general. This is reflected by density of the electric fields not exponentially decay in normal distance from the electrodes (Figure 8.a), distribution of electric field over plane really not circular between electrodes (Figure 8.b) and the complete absence of strongly edge-coupled field distribution (high density concentration around edges and scarce in inner electrode regions) missing in the modelling (meaning of approximation with low details in the modelling). Furthermore, the presented results are restrained to be informative and descriptive for static test results over time. So, there are no implications on skin-effect arising from the varied frequency of testing voltage and distributed electric field.

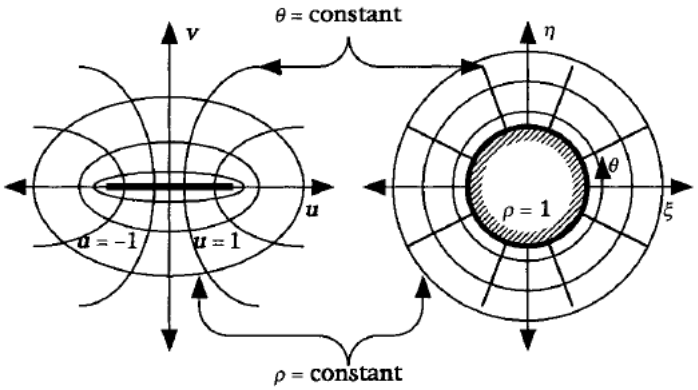

FIGURE 7. SIDE VIEW OF MICROSTRIP-LINE CONDUCTORS FOR CONFORMAL MAPPING TO DEFINE SOLUTION FOR BENDING ELECTRICAL FIELD OVER PLANAR STRIP-LINE CONDUCTORS AND COPLANAR ELECTRODES [98].

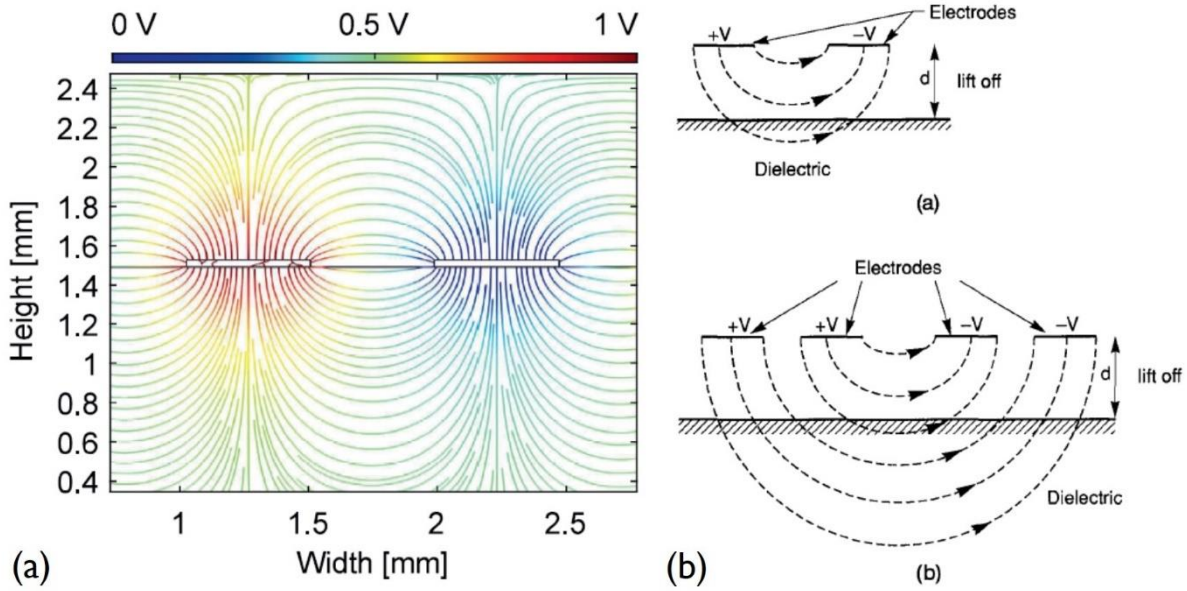

FIGURE 8. APPROXIMATE DISTRIBUTION OF ELECTRIC FIELD OVER AND POTENTIAL DROP BETWEEN DIFFERENT POLARISED COPLANAR ELECTRODES (A)[99]. ILLUSTRATION OF VARIED PENETRATION DEPTH OF ELECTRIC FIELD ACCORDING TO DIFFERENT GAP SIZE BETWEEN ELECTRODES (B) [100].

Derivation of resistive and capacitive components of tested materials can be performed by various methods as there are multiple solutions in the literature for DC and average, stationer type AC test results. To arrive for proper closed formulas to define the main physical parameters require eloquent mathematical knowledge and skills, far more than as described in simple expressions in the literature [101–103]. Although exact solution of the Poisson and Laplace equations with Dirichlet boundary conditions can be solved [104,105], modern FEM solver tools can also provide accurate estimations [106–108] especially useful for complex structures [109] but it requires elaborate preparation for modelling. To perform rapid and sufficiently accurate assessment, closed expressions are also available in the literature. In the following, two appropriate methods are described to mathematically model response of interdigitated electrodes and the results compared to each other. Material resistivity and capacitance is calculated using the cell constant (K_{cell}) as given in the following Equations 1 and 2. In addition, resistance derivation from measurement results is given in Equation 3.

$$R = \frac{K_{cell}}{R_{coat}} \qquad Equation\ 1$$

$$C_{cell} = \frac{\epsilon_o \times \epsilon_r}{K_{cell}} \qquad Equation\ 2$$

$$R = \rho \times k \quad . \qquad Equation\ 3$$

The proportionality factor, cell constant (m^{-1}) of the IDE expresses ratio between the sensor active surface area and penetration depth of the electrical field, effective cross-section of the tested material. Thus, specific resistance (ρ, ohm m) multiplied with the cell constant returns measured resistance (R, ohm) and in turn measured resistance divided by cell constant gives actual specific resistance of the tested coating. According to the literature, there are number of ways to define cell constant of interdigitated electrodes for variety of materials and test conditions. Furthermore, in part of the solution, majority of capacitive assessment includes elliptical integrals to calculate normal component and charge accumulation by the electrical field. Capacitance was estimated for the IDE-0.55 and IDE-1.1 prototypes based on one of the most recent literature example [110]. Using a multiplication factor of 4.3 as relative permittivity of the polyimide sensor substrate, 1.154×10^{-10} F capacitance is expected to measure with both sensors due to the same geometrical ratio of width of and gap between strip-line electrodes. This normalised to unit length (1 m) of the sensor electrodes becomes equal with 2.912×10^{-11} F/m. Estimated cell constants were around 0.251 for both sensor electrodes. Experimental results showed acceptable match especially in regard with the thin blocking layer of polyimide covered both sides of the prototypes over active electrode areas in the closest, the most sensitive sensor volume range. Theoretical, experimental and derived results are summarised in

Table 2 (page 23).

When IDE type sensors are used for detection of insulating materials, then the lowest cell constant is favourable in order to maximise sensitivity of detection. In other words, larger active electrode surface via greater electrode length is preferred to formulize over unit surface area. Such sensors with a length of 5.2 m compared to the very small electrode width and gap (0.55 and 1.1 mm) is unparalleled in the literature. This means if such a probe may fail at detection sensitivity with testing high resistive maritime coatings, then most probably there must be no point in making any further attempts to accommodate the IDE sensor option in sensor development program of the DTP.

TABLE 2. THEORETICAL, EXPERIMENTAL AND DERIVED MATERIAL PROPERTIES OF THE IDE TYPE SENSOR PROTOTYPES

Derived material properties	Sensor electrode types	
Theoretical	IDE-0.55	IDE-1.1
Capacitance (F)	1.154×10^{-10}	1.154×10^{-10}
Cell constant (m^{-1})	0.251	0.251
Experimental (under air)		
Capacitance (F)	2.52×10^{-10}	2.13×10^{-10}
Cell constant (m^{-1})	0.151	0.179

Other most recent capacitance calculation based cell constant estimation of IDE strip lines [111] lead to similar results which listed in Table 3. As it seems, simpler expressions lead to estimations some overestimation of material capacitive properties but in this case differentiation was obtained with the varying geometry of the IDE sensors. Thus, if estimation by closed expression used to optimise geometry of the IDE sensors in an early design stage, then experimental validation is certainly advised and highly recommended.

TABLE 3. THEORETICAL, EXPERIMENTAL AND DERIVED PROPERTIES OF THE IDE TYPE SENSOR PROTOTYPES

Estimated material properties	Sensor electrode types	
	IDE-0.55	IDE-1.1
Capacitance under air (F)	1.4×10^{-10}	1.12×10^{-10}
Capacitance with tested material (ε_r = 5, F)	1.63×10^{-10}	1.30×10^{-10}
Sum of capacitance (F)	3.04×10^{-10}	2.41×10^{-10}
Cell constant (m^{-1})	0.271	0.341

In comparison with the concentric array type prototype, the resistance of the IDE sensors is markedly low and capacitive base signals were high in similar proportion. This is in agreement with the much larger length of the edge-coupled electrodes and the equal or around half of the electrode gap with the IDE-0.55 sensor. In the subsequent section, the concentric array sensor is discussed.

5.2 The concentric array sensor

To counteract part of the shortages featured by open-ended microstrip-line sensors, concentric electrode configurations were introduced. Front-side view of a small section of disk-ring type concentric array electrical conductivity sensor is presented in Figure 9.

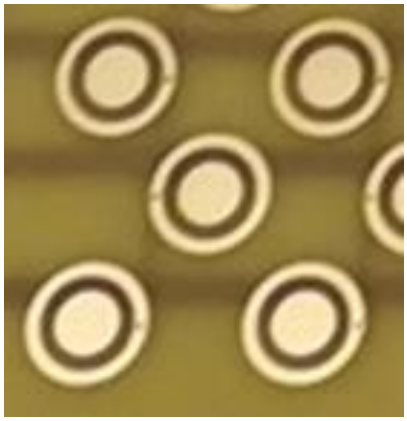

FIGURE 9. FRONT-SIDE VIEW OF A CONCENTRIC ARRAY TYPE ELECTRICAL CONDUCTIVITY SENSOR.

Similarly to the aforementioned details of calculating exact trans-capacitance response signal of such sensors require dedicated mathematical approach or proper detail of FEM can also be proper alternative. When model and FEM solver is properly established in detail, then calculation results must provide output on potential distribution between and around the concentric electrodes as it seems in Figure 10.a and b. Former part of the figure indicates variation of potential amplitude in-plane over the sensor surface when the outer ring electrode is electrified for material testing (three images on left hand side, Figure 10.a), whereas images on the right hand side in Figure 10.b indicates potential distribution when inner disk electrode excited for sensing. The impact of edge coupled disk-ring electrodes is obviously reflected from the simulation results indicating high voltage amplitude between volume range of the electrodes, rapidly decaying over inner electrode areas (Figure 10.a). It also obvious, voltage perturbation, material testing can be far more sensitive by using the outer ring electrode as a driver rather than the smaller size inner disk for material electrification. This can be immediately understood by contemplating the huge difference between covered volume ranges by the two electrode coupling cases, i.e., driver outer and sense inner (Figure 10.a), driver inner and sense outer (Figure 10.b). The former is far more sensitive and so favourable than the latter. More on the advantage obtained by the proper electrode coupling for material testing, to couple the outer electrode for driving (to proper voltage perturbation and electronification) herewith provides effective, controlled overriding voltage signal, shielding from EMI noise signals coming from the environment. Then, the sense electrode always measure part of the trans-capacitance signal affected by the volume range between the ring-disk electrodes. Although the presented simulation results can be considered to be above the average, these are still far not regarded as full-scale solution to sensor application due to missing validated capacitive response signal as a function of material properties and extensive solution space to describe expected impedance test results. Skin-effect generally leads to intense shrinkage of tested volume range of materials with the increasing frequency of voltage signal while frequency distortion of the measured current signal is directly information on system, material properties.

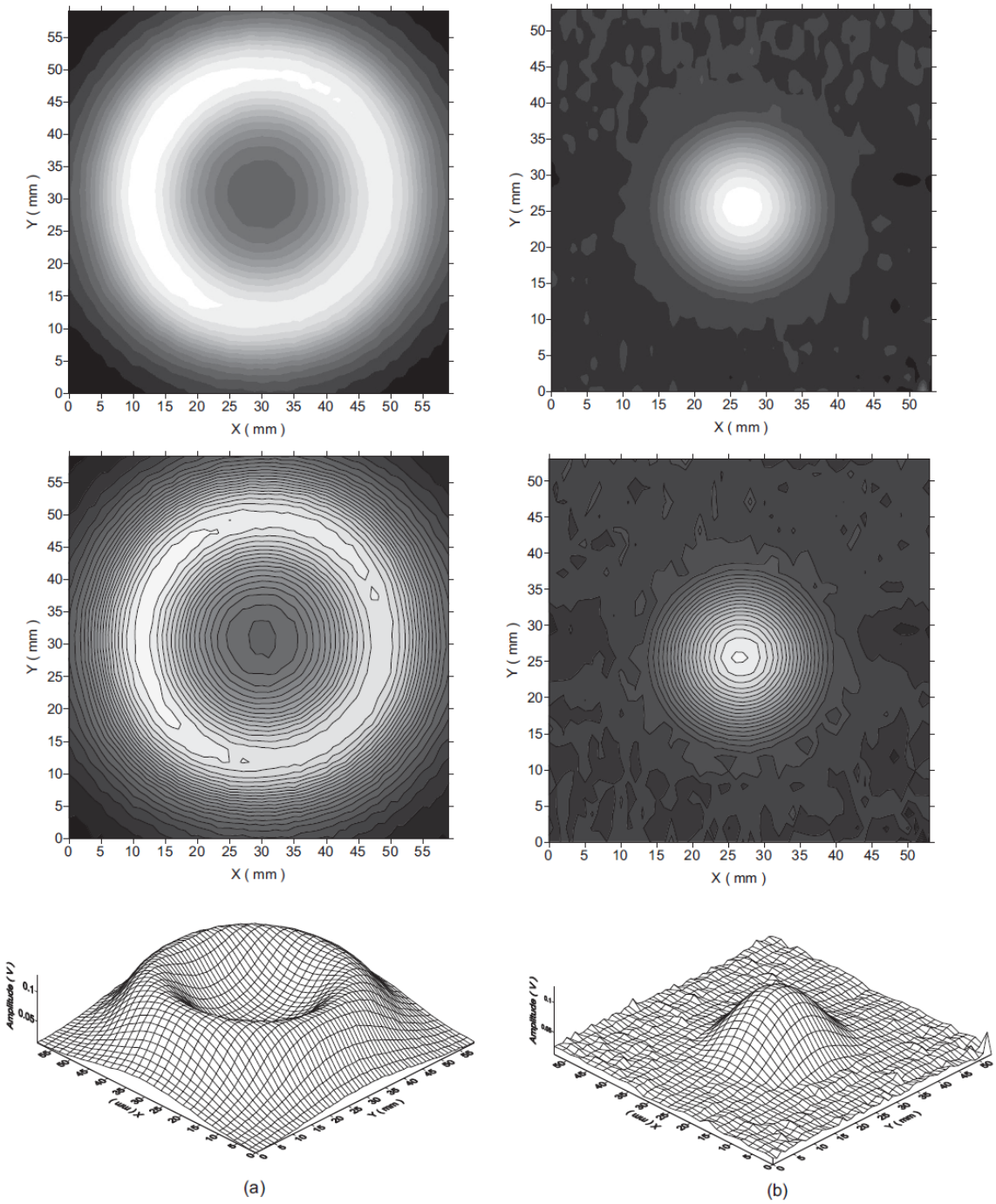

FIGURE 10. ELECTRIC FIELD DISTRIBUTION PLOTS OF IMPRESSED CONCENTRIC RING ELECTRODES SENSOR CONFIGURATION BASED ON DETAILED FEM, WHEN THE OUTER RING (A) AND THE INNER DISK ELECTRODES (B) ARE DRIVEN (SUPPLIED) WITH VOLTAGE FOR ELECTRIFICATION OF TESTED MATERIALS [112].

Based on literature findings, sensitivity by the concentric and semi-concentric probes is superior to strip-line configurations [113]. In addition, insulation performance assessment is advised to perform with concentric probes, disk−ring electrodes, according to standard recommendations [114−120]. Industrial examples offer surface/volume concentric ring probes measuring within the resistivity range of 10^3 and 10^{13} ohm by using test voltage of 10−100 V when measured current at 13 mA and 1.7 mA, respectively [121]. Special electrode configurations are in compliance with the ASTM

D257 [114], ANSI/ESD STM11.11 [122] and STM11.12 [123] standards. The concentric array of spring-loaded pin probes with variety of pin-head configurations, e.g., 'ETS Model 8' series resistance/resistivity probes' by Electro-tech Systems, Inc offers the potential for continuous monitoring rather operating in inspection use case [124]. As a further step in customisation, miniaturised concentric pin-arrays, i.e., the PRF-912B Miniature E12 Micro Probe Set by Prostat® Corporation [125] are constructed to offer accurate surface resistance assessment over small areas in a remarkably wide resistance range between 1 and 10^{12} ohm. The latter corresponds to upper limit of coating resistance in very good condition at naval vessels.

Surface resistivity (ρ) and capacitive properties (*CPE*) of tested materials, i.e., paint coatings with thickness of up to 1 mm, is derived from DC and AC measurement results of surface resistance (R) as given in the following. First, the cell constant (k) and the single probe solution is expressed. Then, it is extended to arrays with arbitrary number of probes via using calculated normalising correction factors which is given subsequently. The cell constant k is calculated as expressed in Equation 4:

$$k = \frac{2\pi}{ln\left(\frac{r_2}{r_1}\right)} \qquad \text{EQUATION 4}$$

where r_2 and r_1 are the inner and outer radius of ring and disk electrodes of a single probe, respectively. As a 2 dimensional segment of cylindrical structure, this dimensional factor expresses the ratio of length and distance between the inner and outer sensor electrodes. This simplification to purely 2 dimensional conduction mechanism and neglection of any marked conductivity contribution from the 'bulk' region in case of thick coatings generally provides a good estimation. Explicit derivation of overall surface resistance (R) is a multiplication with the cell constant (k) and the sum of surface (A) confined with the ring-disk electrodes (Equation 5).

$$\rho = R \times k \times A \qquad Equation\ 5$$

Thus, array extension related correction is given by sum of electrode covered surface area and so surface resistivity of the coatings (ρ) equals with DC extrapolated resistance extraction from the impedance spectra or ratio of testing voltage and measured current (according to the Ohm's law) obtained from chrono-amperometry, chronopotentiometry and potentiostatic measurement results. The sum of surface area of tested materials, paint coating is given in Equation 6.

$$A = \pi \times (r_2^2 - r_1^2) \times n \qquad Equation\ 6$$

Advantage of this resistance characterisation, condition assessment becomes easy to understand and interpretate sensor readings by maintenance experts, technicians and possibly crew members. In addition, this provides the chance and in case of need for contingent trouble shooting relating to surface installation of the sensors based on possibly erroneous measurement results which can also be noticed and rectified by less trained maintenance personnel. In the aspects of sensor optimisation, the cell constant is a key factor to ensure close surface area of the driver and sense electrodes while keeping size of the single cell low and so to assure moderate lateral extent of the arrays. Furthermore, an electrode gap is required to be at least comparable with thickness of the coatings to ascertain sufficient penetration depth into coatings to gain around full cross-sectional assessment. The concentric array prototype was designed to feature a cell constant of 15.5 (recommended for wide-range resistivity assessment) with an overall surface area of 141.4 cm^2 (between the electrodes) by utilising 900 individual probes in lateral distribution of 25 times of 36 in length and width. After the correction, dimension of the surface resistance becomes conform with general standard of ohm cm^2. The many probes with limited maximum testing voltage

of 1 V ascertains confident detection of current at least 3 times above the minimum threshold of majority of the mobile and laboratory test equipment (0.1 nA) applicable to naval coatings with specific resistance of up to 2.5×10^{14} ohm m. The latter may seem to be excessive as this range corresponds to excellent coating condition which can obviously be the case within the first two years of service after entirely new paint application. In another viewpoint, this is far not the interested resistance range by the experts to facilitate organisation of maintenance actions. Therefore, this means redundancy in the prototype for current detection offers the chance to reduce the number of probes and so decrease original lateral size of the sensor laminate (322 × 272 cm). Normalisation of the CPE component is to be performed by the set of same correction factors but in this case division must be applied (instead of multiplication) as stated in Equation 7.

$$CPE_{norm} = \frac{CPE_{meas}}{k \times A} \qquad \text{EQUATION 6}$$

Thus, dimension of data can be expressed as $ohm^{-1}\ cm^{-2}\ s^{n}$ or $F\ cm^{-2}\ s^{n-1}$. Further transformation to data featuring idealised theoretical capacitive property in dimension of $F\ cm^{2}$ needs further correction based on frequency of data extraction from spectra as stated in Equation 5 in which Z_C stands for absolute capacitance of an ideal capacitive element (valid without resistance at a certain frequency) and Z_{CPE} stands for impedance of a real capacitor vs angular frequency range. The maximum featuring frequency is the normalising frequency for data to be normalised over the frequency range (Equation 8).

$$Z_C = \frac{1}{C} \times \frac{1}{\omega} = \frac{1}{Y_o} \times \frac{1}{\omega^n} = Z_{CPE} \qquad \text{EQUATION 7}$$

Combination of the Cole-Cole type impedance [126,127] with parallel coupled resistive and capacitive type elements leads to angular frequency independent expression as stated in Equations 9 and 10.

$$Y_o = R^{n-1}C^n \qquad Equation\ 8$$

$$C = R^{\frac{1-n}{n}} \times Y_o^{\frac{1}{n}} \qquad \text{EQUATION 10}$$

The latter type DeBrug formula [128] offers capacity assessment based on parallel combination of the resistive and capacitive elements. Capacity evaluation by the Randle's arrangement may also result in the same outcome. For details, readers are advised to refer to the appropriate literature [129–131]. Generally, using the CPE data at a frequency of 1/(2×π) can be a good approximation for capacity assessment of coatings, although time constant of some coatings ('black coatings') were usually far below the lowest scanned frequency limit (0.05 Hz).

As partial proof of sensing capability of the concentric array sensor, a comparison is presented in the following. As it seems obvious Figure 11a, coating resistivity character were defined by the concentric array sensor very closely to the range estimated by the traditional setup. The slight difference is due to the always decreasing resistance character of the coating due to the infiltrating aqueous electrolyte. At the beginning of the immersion exposure and coating deterioration, resistive character can be confidently performed by both methods.

On the other hand, the evidence of overestimated coating capacitive character by the wet test setup measured with the PMMA-housed carbon electrodes (PMMA-CE) with filtered sea water becomes plausible even in early stage of testing when compared to test results obtained with prototypes used under dry condition (Figure 11b). An order of magnitude difference is clearly unacceptable, but CPE property is behind the priority to coating resistance in condition assessment.

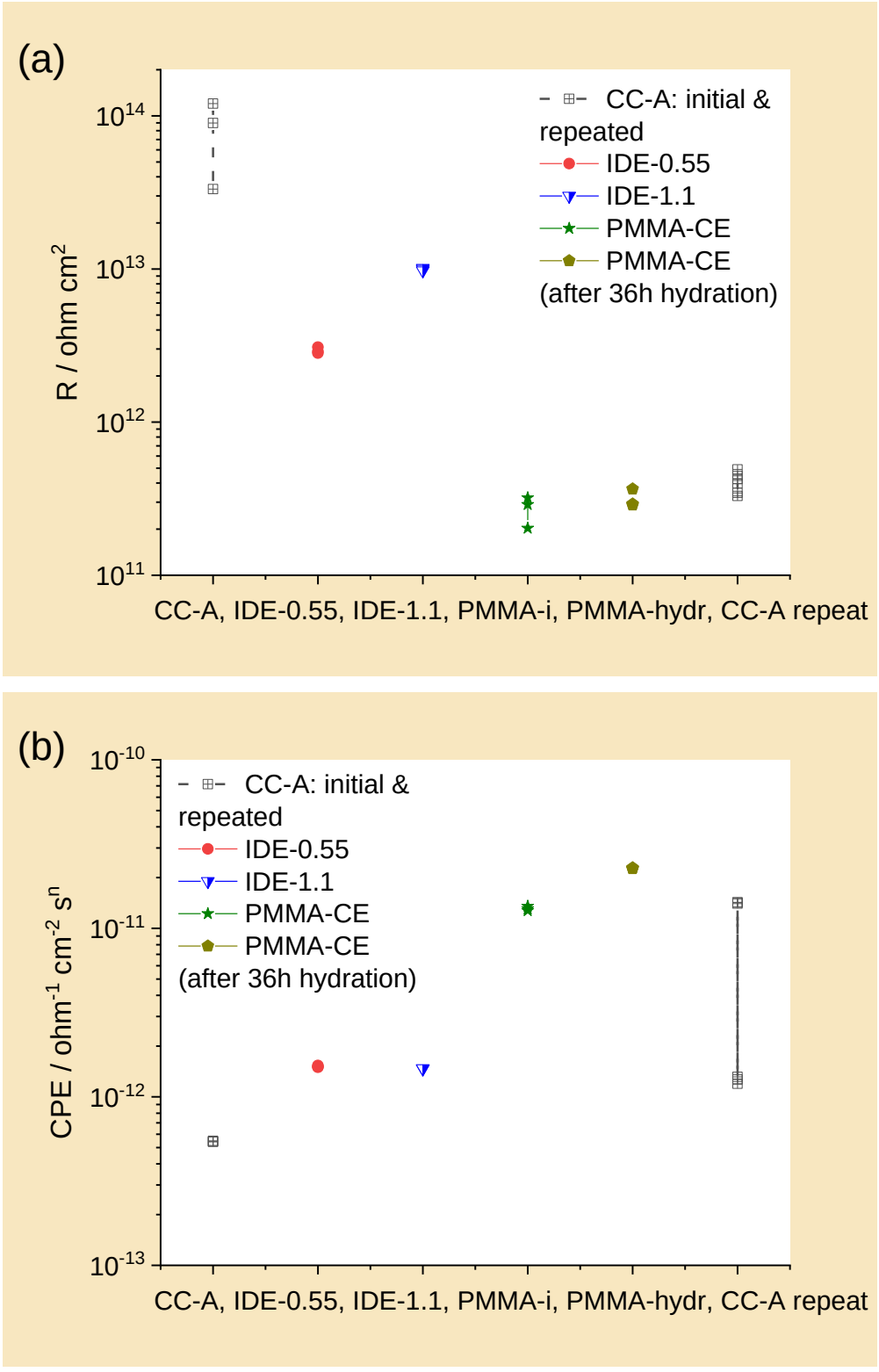

FIGURE 11. COATING RESISTANCE (A) AND THE CONSTANT PHASE ELEMENT (B) DERIVED FROM DATA OBTAINED WITH THE IDE AND CC-A PROTOTYPES, AND THE PMMA-CE PLANAR ELECTRODES ON LONG-TERM IMMERSION TESTED COATING SAMPLE.

6 SUMMARY AND CONCLUSIONS

To summarize the selection process for a suitable coating quality sensor, it can first be stated that wire based electrodes may offer a somewhat more flexible and wider applicability than traditional monolith planar electrodes. However, this is in itself not enough to compensate compromised detection sensitivity and accuracy. In addition, all traditional EIS characterisation require a wet chemistry test mode which has inherent limitations in sensitivity of detection, accuracy and practicability.

Material testing in the dry phase based on fringing electrical field revealed that the open-ended, edge-coupled strip line electrodes provided credible results in the moderate resistance range and to estimate effective permittivity of the materials. Nevertheless, interdigitated sensors did not show promising results with thick, high resistive maritime coatings. In addition, these open electrode configurations proved to be extremely sensitive to outer electromagnetic noise. Therefore, any real-life implementation of such electrode configurations is not recommended both at the maritime and aerospace fields.

In line with the literature, the concentric electrode configuration proved to be superior for sensing due to highly sensitive and robust performance at material characterisation via friending electric field between array of disk-ring and ring-ring probes. It ensures superior sensitivity and accuracy due to the absence of electrolyte, sturdy function against electromagnetic noise which is not scarce at naval ships, and unparalleled high throughput operation which cannot be realised by any other beforementioned test methods. Based on these reasons, the concentric array sensor concept and prototype was decided by DTP experts to be taken in further development, with a targeted customisation for both the maritime and aerospace industry.

REFERENCES

[1] M.T. Gudze, R.E. Melchers, Operational based corrosion analysis in naval ships. Corros Sci 50 (2008) 3296–3307. doi:10.1016/j.corsci.2008.08.048
[2] M. Kendig, S. Jeanjaquet, R. Brown, F. Thomas, Rapid electrochemical assessment of paint. J Coat Technol 68(863):39-47.
[3] J.J. Suay, I.M.T. Rodriguez, R. Izquierdo, A.H. Kudama, J.J. Saura, Rapid assessment of automotive epoxy primers by electrochemical techniques. J Coat Technol 75(946) (2003) 103-111. doi: https://doi.org/10.1007/BF02720157
[4] J.M. McIntyre, H.Q. Pham, Electrochemical impedance spectroscopy; a coatings optimizations. Prog Org Coat 27 (1996) 201-207.
[5] D. Loveday, P. Peterson, B. Rodgers—Gamry instruments, evaluation of organic coatings with electrochemical impedance spectroscopy. JCT Coatings Tech (2005) 22-27.
[6] L.G.S. Gray, B.R. Appleman, EIS: electrochemical impedance spectroscopy, A tool to predict remaining coating life? JPCL (2003) 66-74.
[7] https://www.gamry.com/assets/Application-Notes/REAP.pdf
[8] J.R. Scully, S.T. Hensley, Lifetime Prediction for organic coatings on steel and a magnesium alloy using electrochemical impedance methods. Corrosion 50(9) (1994) 705–716. https://doi.org/10.5006/1.3293547
[9] C.-T. Chen, B.S. Skerry, Assessing the corrosion resistance of painted steel by AC impedance and electrochemical noise techniques. Corrosion 47(8) (1991) 598–611. https://doi.org/10.5006/1.3585298
[10] https://www.emisoftware.com/calculator/wire-pair-capacitance/
[11] B.A. Fellman, Carbon-based electric double layer capacitors for water desalination. MSc Thesis in Mechanical Engineering at the Massachusetts Institute of Technology, Jun 2010.
[12] R. de Levie, On porous electrodes in electrolyte solutions. I. Capacitance effects. Electrochim Acta 8 (1963) 751–780. doi:10.1016/0013-4686(63)80042-0.
[13] R. de Levie, On porous electrodes in electrolyte solutions. Electrochim Acta 8 (1963) 751–780. doi:10.1016/0013-4686(63)80042-0
[14] M. Keddam, C. Rakotomavo, H. Takenouti, Impedance of a porous electrode with an axial gradient of concentration. J Applied Electrochem 14 (1984) 437-448.
[15] S.J. Cooper, A. Bertei, D.P. Finegan, N.P. Brandon, Simulated impedance of diffusion in porous media. Electrochim Acta 251 (2017) 681–689. https://doi.org/10.1016/j.electacta.2017.07.152
[16] J. Huang, Y. Gao, J. Luo, S. Wang, C. Li, Shengli Chen, J. Zhang, Editors' Choice—Review—Impedance response of porous electrodes: theoretical framework, physical models and applications. J Electrochem Soc 167 (2020) 166503. doi: 10.1149/1945-7111/abc655
[17] S.D. Jagtap, S.P. Tambe, R.N. Choudhari, B.P. Mallik, Mechanical and anticorrosive properties of non-toxic coal-tar epoxy alternative coatings. Prog Org Coat 77 (2014) 395–402. http://dx.doi.org/10.1016/j.porgcoat.2013.11.003
[18] M. Sophocleous, Electrical resistivity sensing methods and implications, electrical resistivity and conductivity. A.E. Shahat, IntechOpen, May 31st 2017. doi: 10.5772/67748
[19] F.M. Smits, Measurement of sheet resistivities with the four-point probe. The Bell System Technical Journal (1958) 711-718.
[20] M. Reveil, V.C. Sorg, E.R. Cheng, T. Ezzyat, P. Clancy, M.O. Thompson, Finite element and analytical solutions for van der Pauw and four-point probe correction factors when multiple non-ideal measurement conditions coexist. Rev Sci Instrum 88 (2017) 094704. https://doi.org/10.1063/1.5001830
[21] S.H.N. Lim, D.R. McKenzie, M.M.M. Bilek, van der Pauw method for measuring resistivity of a plane sample with distant boundaries. Rev Sci Instrum 80 (2009) 075109. https://doi.org/10.1063/1.3183503

[22] S.P. Kikken, Measuring film resistivity understanding and refining the four-point probe set-up. BSc Thesis at the Eindhoven University of Technology, 2018.
[23] C. Kasl, M.J.R. Hoch, Effects of sample thickness on the van der Pauw technique for resistivity measurements Rev Sci Instrum 76 (2005) 033907. https://doi.org/10.1063/1.1866232
[24] F. Werner, Hall measurements on low-mobility thin films. J Appl Phys 122 (2017) 135306. https://doi.org/10.1063/1.4990470
[25] W.C. Heerens, Application of capacitance techniques in sensor design. Review article. J Phys E: Sci Instrum 19 (1986) 897-906.
[26] ASTM D877 / D877M-19, Standard test method for dielectric breakdown voltage of insulating liquids using disk electrodes, ASTM International, West Conshohocken, PA, 2019, www.astm.org doi: 10.1520/D0877_D0877M-19
[27] S. DARAYAN, D.P. SHATTUCK, L.C. SHEN, R.C. LIU, MEASUREMENT OF DIELECTRIC CONSTANT AND CONDUCTIVITY OF SAMPLES USING GUARDED ELECTRODES. IEEE XPLORE 31(6) (1996) 1417–1426. DOI: 10.1029/96RS01728
[28] M. Lisowski, R. Kacprzyk, Changes proposed for the IEC 60093 Standard concerning measurements of the volume and surface resistivities of electrical insulating materials. 13(1) (2006) 139–145. doi: 10.1109/TDEI.2006.1593412
[29] B.A. Mazzeoa, A.J. Flewitt, Two- and four-electrode, wide-bandwidth, dielectric spectrometer for conductive liquids: Theory, limitations, and experiment. J Appl Phys 102 (2007) 104106. https://doi.org/10.1063/1.2815666
[30] P.B. Ishai, M.S. Talary, A. Caduff, E. Levy, Y. Feldman, Electrode polarization in dielectric measurements: a review. Meas. Sci. Technol. 24 (2013) 102001 (21pp). doi:10.1088/0957-0233/24/10/102001
[31] W.C. CHEW, J.A. KONG, EFFECTS OF FRINGING FIELDS ON THE CAPACITANCE OF CIRCULAR MICROSTRIP DISK. IEEE TRANS MICROW THEORY TECH 28(2) (1980) 98-104. DOI: 10.1109/TMTT.1980.1130017
[32] W.C. Chew, J.A. Kong, Microstrip capacitance for a circular disk through matched asymptotic expansions. Siam J Appl Math 42(2) (1982) 302-317. doi: https://doi.org/10.1137/0142024
[33] C. Freye, F. Jenau, Model-based accuracy enhancements for guarded conductivity measurements: determination of effective electrode areas utilising numerical field simulation. High Volt 3(3) (2018) 217-225. doi: 10.1049/hve.2017.0182
[34] T.J. Higgins, D.K. Reitan, Calculation of the capacitance of a circular annulus by the method of subareas. AIEE Transactions 70 (1951) 926-933.
[35] D. Kołakowska, M. Lisowski, The effective area of measurement electrode in volume resistivity and permittivity of solid dielectrics measurements. Meas Autom Montrg 61 (2015) 32-34.
[36] E.A. Stricker, X. Ke, J.S. Wainright, R.R. Unocic, R.F. Savinell, Current density distribution in electrochemical cells with small cell heights and coplanar thin electrodes as used in EC-S/TEM cell geometries. J Electrochem Soc 166(4) (2019) H126-H134. doi: 10.1149/2.0211904jes
[37] Z. Chen, R.C. Luo, Design and Implementation of capacitive proximity sensor using microelectromechanical systems technology. IEEE Trans Ind Electron 45(6) (1998) 886-894. doi: 10.1109/41.735332
[38] I.J. Bahl, Stanislaw S. Stijchly, Analysis of a microstrip covered with a lossy dielectric. IEEE Trans Microw Theory Techn 28 (2) (1980) 104-109.
[39] T. Chen, J.R. Bowler, N. Bowler, Analytical solution for capacitance calculation of a curved patch capacitor that conforms to the curvature of a homogeneous cylindrical dielectric rod. Appl Phys Lett 104 (2014) 032901. doi: 10.1063/1.4862434
[40] V. Novickij, A. Tabasnikov, S. Smith, A. Grainys, J. Novickij, Analysis of planar circular interdigitated electrodes for electroporation. IETE Tech Rev (2015) 1-7. doi: 10.1080/02564602.2014.1000982
[41] T. Chen, N. Bowler, Design of interdigital spiral and concentric capacitive sensors for materials evaluation. AIP Conf Proc 1511 (2012): 1593–1600. http://dx.doi.org/10.1063/1.4789232.
[42] T. Chen, Capacitive sensors for measuring complex permittivity of planar and cylindrical structures. PhD Thesis at the Iowa State University, Ames, Iowa 12294, (2012). https://lib.dr.iastate.edu/etd/12294.

[43] A.V. Mamisheva, A.R. Takahashib, Y. Duc, B.C. Lesieutred, M. Zahn, Parameter estimation in dielectrometry measurements. J Electrostat 56 (2002) 465–492. https://doi.org/10.1016/S0304-3886(02)00068-2
[44] C.-U. Kim, G. Li, J. Li, H. Jong, C. Ro, Y. Song, G. Pak, S. Im, Numerical analysis on effective electric field penetration depth for interdigital impedance sensor. J Phys Conf Ser 418 (2013) 012020. doi:10.1088/1742-6596/418/1/012020
[45] R. Karthik, V. Tummala, Voltage dependent Maxwell-Wagner polarization in dielectric heterostructures. Mater Today Proc 4 (2017) 8751–8757. https://doi.org/10.1016/j.matpr.2017.07.224
[46] T.C. Chapman, H.J. Wintle, Dielectric absorption currents and surface charge on polymeric insulators. J Appl Phys 51 (1980) 4898. doi: 10.1063/1.328328
[47] J.K. Jeszka, J. Ulanski, I Glowacki, M. Kryszewski, Surface component of absorption and resorption currents in polymethyl methacrylate and polystyrene In different conditions: thermally stimulated resorption. J Electrostatics 16 (1984) 89-98.
[48] X.B. Li, S.D. Larson, A.S. Zyuzin, A.V. Mamishev, Design principles for multichannel fringing electric field sensors. IEEE Sensors Journal 6(2) (2006) 434-440. doi: 10.1109/JSEN.2006.870161
[49] P. Xiao, H. Singh, X. Ou, A.R. Caparnagiu, G. Kramer, RE. Imhof, In-vivo Solvent Penetration Measurement using Contact Imaging and Skin Stripping. Poster Presentation, SCC Technology Showcase, New York 2011.
[50] X. Huang, W.-H. Yeo, Y. Liu, J.A. Rogers, Epidermal differential impedance sensor for conformal skin hydration monitoring. Biointerphases (2012) 7:52. doi:10.1007/s13758-012-0052-8
[51] E. Xhauflaire-Uhoda, G. Mayeux, P. Quatresooz, A. Scheen, G.E. Piérard, Facing up to the imperceptible perspiration. Modulatory influences by diabetic neuropathy, physical exercise and antiperspirant. Skin Res Technol 17(4) (2011) 487-493. doi: 10.1111/j.1600-0846.2011.00523.x
[52] E. Xhauflaire-Uhoda, C. Piérard-Franchimont, G.E. Piérard, Skin capacitance mapping of psoriasis. JEADV 20 (2006) 1261-1265. doi: 10.1111/j.1468-3083.2006.01787.x
[53] X. Zhang, C. Bontozoglou, E. Chirikhina, M.E. Lane, P. Xiao, Capacitive imaging for skin characterizations and solvent penetration measurements. Cosmetics 5 (2018) 52. doi:10.3390/cosmetics5030052
[54] P.F. Laleicke, F.A. Kamke, A capacitive multi-wavelength sensor for moisture content gradient sensing in wood. Wood Sci Technol 52 (2018) 717–732. https://doi.org/10.1007/s00226-018-0988-z
[55] P. Clarys, A.O. Barel, Chapter 15 Measurement of skin surface hydration in P. Humbert et al. (eds.), Agache's measuring the skin. Springer International Publishing Switzerland, 2017. doi:10.1007/978-3-319-32383-1_15
[56] H. Singh, Development of a measurement instrument using capacitance sensors techniques to image and measure the skin surface hydration. London South Bank University, November 2010.
[57] A. Orangi, G.A. Narsilio, D. Ryu, A laboratory study on non-invasive soil water content estimation using capacitive based sensors. Sensors 19 (2019) 651. doi:10.3390/s19030651
[58] J. Hu, M. Jiang, X. Zhao, Z. Lin, Fringing field sensor using a circuit-modulated parameter for measuring water content in a soil sample. J Irrig Drain Eng 134 (2008) 356-360. doi: 10.1061/(ASCE)0733-9437(2008)134:3(356)
[59] M.S. us Sarwar, Soft capacitive sensors for proximity, touch, pressure and shear measurements. PhD Thesis at the University of British Columbia, Vancouver, 2019.
[60] T.D. Nguyen, H.S. Han, H.-Y. Shin, C.T. Nguyen, H. Phung, H. van Hoang, H.R. Choi, Highly sensitive flexible proximity tactile array sensor by using carbon micro coils. Sens Actuators A 266 (2017) 166–17. http://dx.doi.org/10.1016/j.sna.2017.09.013 0924-4247/
[61] B. Tsai, E. Birgersson, U. Birgersson, Mechanistic multilayer model for non-invasive bioimpedance of intact skin. J Electr Bioimp 9 (2018) 31-38. https://doi.org/10.2478/joeb-2018-0006
[62] B. Tsai, H. Xue, E. Birgersson, S. Ollmar, U. Birgersson, Analysis of a mechanistic model for non-invasive bioimpedance of intact skin. J Electr Bioimp 8 (2017) 84-96. https://doi.org/10.5617/jeb.4826
[63] T. Chen, N. Bowler, Analysis of a concentric coplanar capacitive sensor for nondestructive evaluation of multi-layered dielectric structures. IEEE Trans Dielectr Electr Insul 17(4) (2010) 1307-1318.

[64] K. Wang, U. Parekh, T. Pailla, H. Garudadri, V. Gilja, T.N. Ng, Stretchable dry electrodes with concentric ring geometry for enhancing spatial resolution in electrophysiology. Adv Healthcare Mater (2017) 1700552. doi: 10.1002/adhm.201700552
[65] S. Nebuya, M. Noshiro, B.H. Brown, R.H. Smallwood, P. Milnes, Detection of emboli in vessels using electrical impedance measurements—phantom and electrodes. Physiol Meas 26 (2005) S111–S118. doi:10.1088/0967-3334/26/2/011
[66] J. Garcia-Casado, Y. Ye-Lin, G. Prats-Boluda, O. Makeyev, Evaluation of bipolar, tripolar, quadripolar Laplacian estimates of electrocardiogram via concentric ring electrodes. Sensors 19 (2019) 3780. doi:10.3390/s19173780
[67] G. Prats-Boluda, Y. Ye-Lin, E. Garcia-Breijo, J. Ibanez, J. Garcia-Casado, Active flexible concentric ring electrode for non-invasive surface bioelectrical recordings. Meas Sci Technol 23 (2012) 125703 (10pp) doi:10.1088/0957-0233/23/12/125703
[68] X.B. Li, V.V. Inclan, G.I. Rowe, A.V. Mamishev, CEIDP '05. 2005 Annual Report Conference on Electrical Insulation and Dielectric Phenomena, 2005. IEEE Xplore (2005) 617-620. doi: 10.1109/CEIDP.2005.1560758
[69] W.G. Besio, K. Koka, R. Aakula, W. Dai, Tri-polar concentric ring electrode development for laplacian electroencephalography. IEEE Trans Biomed Eng 53 (2006) 926-933. 10.1109/TBME.2005.863887
[70] G. Prats-Boluda, Y. Ye-Lin, J. Bueno-Barrachina, R. Rodriguez de Sanabria, J. Garcia-Casado, Towards the clinical use of concentric electrodes in ECG recordings: influence of ring dimensions and electrode position. Meas. Sci. Technol. 27 (2016) 25705 (11p). doi:10.1088/0957-0233/27/2/025705
[71] S.M. Lee, J.H. Kim, H.J. Byeon, Y.Y. Choi, K.S. Park, S. Lee, Stretchable dry electrodes with concentric ring geometry for enhancing spatial resolution in electrophysiology. J Neural Eng 10 (2013) 36006. doi: 10.1002/adhm.201700552
[72] C.T. Lin, L. De Liao, Y.H. Liu, I.J. Wang, B.S. Lin, J.Y. Chang, Novel dry polymer foam electrodes for long-term EEG measurement. IEEE Trans Biomed Eng 58 (2011) 1200-1207. 10.1109/TBME.2010.2102353
[73] Z. Ren, Exploration of medical applications of electrical capacitance tomography. PhD Thesis, at the Faculty of Engineering and Physical Science, University of Manchester, 2015.
[74] R.C. Luo, Z. Chen, Modeling and implementation of an innovative micro proximity sensor using micromachining technology. Proceedings of 1993 IEEE/RSJ International Conference on Intelligent Robots and Systems (IROS '93). IEEE Int Conf Int Rob Sys, Yokohama, Japan (1993) 1709-1716. **doi:** 10.1109/IROS.1993.583867
[75] M. Ibrahim, J. Claudel, D. Kourtiche, M. Nadi, Chapter 1, Geometric parameters optimization of planar interdigitated electrodes for bioimpedance spectroscopy. J Electr Bioimpedance 4 (2017) 13–22. doi:10.1088/978-0-7503-1505-0ch1
[76] T. Islam, S.C. Mukhopadhayay, Chapter 1, Wearable sensors for physiological parameters measurement: physics, characteristics, design and applications. Wearable Sens Appl, Des Implemn (2017) 1-31. doi:10.1088/978-0-7503-1505-0ch1
[77] Y. Liu, Y. Liang, L. Xue, R. Liu, J. Tao, D. Zhou, X. Zen, Polystyrene-coated interdigitated microelectrode array to detect free chlorine towards IoT applications. Anal Sci 35(5) (2019) 505-509. https://doi.org/10.2116/analsci.18P460
[78] J.S. Kim, D.G. Lee, Analysis of dielectric sensors for the cure monitoring of resin matrix composite materials. Sens Actuators B 30 (1996) 159-164.
[79] O. de Andrade Raponia, R. de Andrade Raponib, G.B. Barbana, R.M. di Benedettoa, A.C. Ancelotti Jr, Development of a simple dielectric analysis module for online cure monitoring of a commercial epoxy resin formulation. Mater Res 20 (Suppl. 2) (2017) 291-297. doi: http://dx.doi.org/10.1590/1980-5373-MR-2017-0067
[80] A.J. Bur, S.C. Roth, Y.-H. Lee, M. McBrearty, A dielectric slit die for in-line monitoring of polymer compounding. Rev Sci Instrum 75 (2004) 1103. doi: 10.1063/1.1667256
[81] E. Schindelholz, R.G. Kelly, I.S. Cole, W.D. Ganther, T.H. Muster, Comparability and accuracy of time of wetness sensing methods relevant for atmospheric corrosion. Corros Sci 67 (2013) 233–241. http://dx.doi.org/10.1016/j.corsci.2012.10.026

[82] Q.N. Minh, H. D. Tong, A. Kuijk, F. van de Bent, P. Beekman, C.J.M. van Rijn, Gas sensing performance at room temperature of nanogap interdigitated electrodes for detection of acetone at low concentration. RSC Adv 7 (2017) 50279. doi: 10.1039/c7ra09441h
[83] J. Sears, Interdigital dielectrometry based detection and identification of dangerous materials for security applications. MSc at the Massachusetts Institute of Technology, Massachusetts Institute of Technology, 2003.
[84] P. Tomčík, Microelectrode arrays with overlapped diffusion layers as electroanalytical detectors: theory and basic applications. Sensors 13 (2013) 13659-13684. doi:10.3390/s131013659
[85] H. Sadeghian, Y. Hojjat, M. Soleimani, Interdigitated electrode design and optimization for dielectrophoresis cell separation actuators. Journal of Electrostatics 86 (2017) 41-49. http://dx.doi.org/10.1016/j.elstat.2017.01.012
[86] D.H. Huynh, Novel Applications of static micro-scale interdigitated electrodes for energy harvesting and biosensing. PhD Thesis at the Department of Electrical and Electronic Engineering School of Engineering, The University of Melbourne, 2017.
[87] K.J. Latimer, J.W. Evans, M.A. Cowell, P.K. Wright, Modeling of interdigitated electrodes and supercapacitors with porous interdigitated electrodes. J Electrochem Soc 164(4) (2017) A930-A936. doi: 10.1149/2.0061706jes
[88] S. Partel, S. Kasemann, V. Matylitskaya, C. Thanner, C. Dincer, G. Urban, A simple fabrication process for disposable interdigitated electrode arrays with nanogaps for lab-on-a-chip applications. Microelectron Eng 173 (2017) 27–32. http://dx.doi.org/10.1016/j.mee.2017.03.014
[89] V. Matylitskaya, S. Kasemann, G. Urban, C. Dincer, S. Partel, Electrochemical characterization of nanogap interdigitated electrode arrays for lab-on-a-chip applications. J Electrochem Soc 165(3) (2018) B127-B134. doi: 10.1149/2.0701803jes
[90] A. Guimerà, G. Gabriel, E. Prats-Alfonso, N. Abramova, A. Bratov, R. Villa, Effect of surface conductivity on the sensitivity of interdigitated impedimetric sensors and their design considerations. Sensors and Actuators B 207 (2015) 1010–1018. http://dx.doi.org/10.1016/j.snb.2014.10.134
[91] N. Couniot, A. Afzalian, N. van Overstraeten-Schlögel, L.A. Francis, D. Flandre, Capacitive biosensing of bacterial cells: Analytical model andnumerical simulations. Sens Actuators B 211 (2015) 428–438. http://dx.doi.org/10.1016/j.snb.2015.01.108
[92] F.N. Toth, A design methodology for low-cost, high-performance capacitive sensors. PhD Thesis at the Technische Universiteit Delft, 1997.
[93] V.K. Tewary, P.R. Heyliger, A.V. Clark, Theory of capacitive probe method for noncontact characterization of dielectric properties of materials. J Mater Res 6(3) (1991) 629-638.
[94] A.V. Mamishev, Y. Du, B.C. Lesieutre, M. Zahn, Development and applications of fringing electric field dielectrometry sensors and parameter estimation algorithms. J Electrostat 46 (1999) 109-123.
[95] X. Yin, D.A. Hutchins, G. Chen, W. Li, Preliminary studies on the design principles of capacitive imaging probes for non-destructive evaluation. Int J Appl Electromagn Mech 42 (2013) 447–470. doi: 10.3233/JAE-131676
[96] B. Stephens-Fripp, V. Sencadas, R. Mutlu, G. Alici, Reusable flexible concentric electrodes coated with a conductive graphene ink for electrotactile stimulation. Front. Bioeng. Biotechnol (2018) https://doi.org/10.3389/fbioe.2018.00179
[97] G. Prats-Boluda, Y. Ye-Lin, F. Pradas-Novella, E. Garcia-Breijo, J. Garcia-Casado, Textile concentric ring electrodes: influence of position and electrode size on cardiac activity monitoring. Hindawi Journal of Sensors Volume 2018, Article ID 7290867, 9 pages https://doi.org/10.1155/2018/7290867
[98] M. Garcia, D. Clague, The 2D electric field above a planar sequence of independent strip electrodes. J. Phys. D: Appl. Phys. 33 (2000) 1747–1755.
[99] J. Döring, L. Tharmakularajah, K.-L. Krieger, Study of interdigital electrode structure for the detection of water spray. 20. GMA/ITG-Fachtagung Sensoren und Messsysteme (2019) 700-707. doi: 10.5162/sensoren2019/P2.7
[100] V.K. Tewary, P.R. Heyliger, A.V. Clark, Theory of capacitive probe method for noncontact characterization of dielectric properties of materials. J Mater Res 6(3) (1991) 629-638.
[101] T.-T. Ngo, A. Bourjilat, J. Claudel, D. Kourtiche, M. Nadi, Design and Realization of a Planar Interdigital Microsensor for Biological Medium Characterization. pp. 23-54, chapter in S.C.

Mukhopadhyay (ed.), Next Generation Sensors and Systems, Smart Sensors, Measurement and Instrumentation 16, ISBN: 978-3-319-21670-6, Springer International Publishing Switzerland 2016, doi: 10.1007/978-3-319-21671-3_2
[102] V. Shtrauss, A. Kalpinsh, U. Lomanovskis, J. Rotbahs, Tomographic imaging by electrical methods, Latvian J. Phys. Tech. Sci., 3 (1995) 23–47.
[103] C.-U. Kim, G. Li, J. Li, H. Jong, C. Ro, Y. Song, G. Pak, S. Im, Numerical analysis on effective electric field penetration depth for interdigital impedance sensor. 7th International Conference on Applied Electrostatics (ICAES-2012) IOP Publishing Journal of Physics: Conference Series 418 (2013) 012020. doi:10.1088/1742-6596/418/1/012020
[104] M. Jamil Amir, M. Yaseen, R. Iqbal, Exact solutions of Laplace equation by differential transform method. (2013) 8 pp. arXiv:1312.7277
[105] T. Fukuchi, High-order accurate and high-speed calculation system of 1D Laplace and Poisson equations using the interpolation finite difference method. AIP Advances 9 (2019) 055312. doi: 10.1063/1.5096395
[106] J. Oberländer, Z.B. Jildeh, P. Kirchner, L. Wendeler, A. Bromm, H. Iken, P. Wagner, M. Keusgen, M.J. Schöning, Study of interdigitated electrode arrays using experiments and finite element models for the evaluation of sterilization processes. Sensors 15 (2015) 26115-26127. doi:10.3390/s151026115
[107] M. Shenouda, D.R. Oliver, Fabrication of an interdigitated sample holder for dielectric spectroscopy of thin films. J Phys Conf Ser 619 (2015) 012028. doi:10.1088/1742-6596/619/1/012028
[108] M. Ibrahim, J. Claudel, D. Kourtiche, M. Nadi, F. Montaigne, G. Lengaigne, Optimization of planar interdigitated electrode array for bioimpedance spectroscopy restriction of the number of electrodes. Fifth Int Conf Sens Technol IEEE Xplore (2011) 612-616.
[109] S. Sathya, S. Muruganand, N. Manikandan, K. Karuppasamy, Design of capacitance based on interdigitated electrode for BioMEMS sensor application. Materials Science in Semiconductor Processing 101 (2019) 206–213. https://doi.org/10.1016/j.mssp.2019.06.005
[110] F.R. Zypman. Mathematical expression for the capacitance of coplanar strips. J Electrostatics 101 (2019) 103371. https://doi.org/10.1016/j.elstat.2019.103371
[111] J. Hrisko, Capacitive soil moisture sensor theory, calibration, and testing. technical report, Maker Portal LLC, New York, NY, July 5 2020. doi: 10.13140/RG.2.2.36214.83522
[112] X. Yin, D.A. Hutchins, G. Chen, W. Li, Preliminary studies on the design principles of capacitive imaging probes for non-destructive evaluation. International Journal of Applied Electromagnetics and Mechanics 42 (2013) 447–470. doi: 10.3233/JAE-131676
[113] R.S. Lima, M.H.D.O. Piazzetta, A.L. Gobbi, T.P. Segato, M.F. Cabral, S.A.S. Machado, E. Carrilho, Highly sensitive contactless conductivity microchips based on concentric electrodes for flow analysis. Chem Commun 49(97) (2013) 11382-11384. doi: 10.1039/C3CC45797D
[114] ASTM D257-14, Standard test methods for DC resistance or conductance of insulating materials, ASTM International, West Conshohocken, PA, 2014, www.astm.org. doi: 10.1520/D0257-14
[115] IEC 60093:1980: 'Methods of test for insulating materials for electrical purposes; volume resistivity and surface resistivity of solid electrical insulating materials', International Electrotechnical Commission Std.
[116] IEC 62631-3-1:2016: 'Dielectric and resistive properties of solid insulating materials – Part 3-1: determination of resistive properties (DC methods) – volume resistance and volume resistivity – general method', International Electrotechnical Commission Std.
[117] IEC 62631-3-2:2015: 'Dielectric and resistive properties of solid insulating materials – Part 3-2: determination of resistive properties (DC methods) – surface resistance and surface resistivity', International Electrotechnical Commission Std
[118] 'DIN IEC 60093:1993-12; VDE 0303-30:1993-12 Prüfverfahren für elektroisolierstoffe; spezifischer durchgangswiderstand und spezifischer oberflächenwiderstand von festen, elektrisch isolierenden Werkstoffen (IEC 60093:1980); Deutsche Fassung HD 429 S1:1983', Deutsche Institut für Normung e.V., Verband der Elektrotechnik Elektronik Informationstechnik e. V. Std.
[119] 'DIN EN 62631-3-1:2017-01; VDE 0307-3-1:2017-01 Dielektrische und resistive Eigenschaften fester Isolierstoffe – Teil 3-1: Bestimmung resistiver Eigenschaften (Gleichspannungsverfahren) – Durchgangswiderstand und spezifischer Durchgangswiderstand – Basisverfahren (IEC 62631-3-

1:2016); Deutsche Fassung EN 62631-3-1:2016', Deutsche Institut für Normung e.V., Verband der Elektrotechnik Elektronik Informationstechnik e. V. Std

[120] 'DIN EN 62631-3-2:2016-10; VDE 0307-3-2:2016-10 Dielektrische und resistive Eigenschaften fester Isolierstoffe – Teil 3-2: Bestimmung resistiver Eigenschaften (Gleichspannungsverfahren) – Oberflächenwiderstand und spezifischer Oberflächenwiderstand (IEC 62631-3-2:2015); Deutsche Fassung EN 62631-3-2:2016', Deutsche Institut für Normung e.V., Verband der Elektrotechnik Elektronik Informationstechnik e. V. Std.

[121] www.trakinc.com

[122] ANSI/ESD - ANSI/ESD STM11.11-2015: SURFACE RESISTANCE MEASUREMENT OF STATIC DISSIPATIVE PLANAR MATERIALS.

[123] ANSI/ESD STM11.12-2015: ESD association standard test method for protection of electrostatic discharge susceptible items - volume resistance measurement of static dissipative planar materials.

[124] https://www.electrotechsystems.com/

[125] www.prostatcorp.com

[126] K.S. Cole, R.H. Cole, Dispersion and absorption in dielectrics I. Alternating current characteristics. J Chem Phys 9 (1941) 341–352. https://doi.org/10.1063/1.1750906

[127] K.S. Cole, R.H. Cole, Dispersion and absorption in dielectrics II. Direct current characteristics. J Chem Phys 10 (1942) 98-105. https://doi.org/10.1063/1.1723677

[128] G.J. Brug, A.L.G. van den Eeden, M. Sluyters-Rehbach, J.H. Sluyters, The analysis of electrode impedances complicated by the presence of a constant phase element. J Electroanal Chem 176 (1984) 275-295. https://doi.org/10.1016/S0022-0728(84)80324-1

[129] C.H. Hsu, F. Mansfeld, Concerning the conversion of the constant phase element parameter Y0 into a capacitance. Corrosion 57/ No. 9 (2001) 747-748. https://doi.org/10.5006/1.3280607

[130] M.R. Shoar Abouzari, F. Berkemeier, G. Schmitz, D. Wilmer, On the physical interpretation of constant phase elements. Solid State Ionics 180 (2009) 922–927. https://doi.org/10.1016/j.ssi.2009.04.002

[131] B. Hirschorn, M. Orazem, B. Tribollet, V. Vivier, I. Frateur, M. Musiani, Determination of effective capacitance and film thickness from constant-phase-element parameters. Electrochim Acta 55 (2010) 6218–6227. doi:10.1016/j.electacta.2009.10.065